Biophysical Journal
Article

Biophysical Society

FERM domains recruit ample PI(4,5)P_2s to form extensive protein-membrane attachments

Thomas Ehret,[1] Tim Heißenberg,[2,3] Svenja de Buhr,[1] Camilo Aponte-Santamaría,[1] Claudia Steinem,[2,3,*] and Frauke Gräter[1,3,4,*]

[1]Heidelberg Institute for Theoretical Studies (HITS), Heidelberg, Germany; [2]Institute of Organic and Biomolecular Chemistry, University of Göttingen, Göttingen, Germany; [3]Max Planck School Matter to Life, Heidelberg and Göttingen, Germany; and [4]Interdisciplinary Center for Scientific Computing (IWR), Heidelberg University, Heidelberg, Germany

ABSTRACT The four-point-one ezrin-radixin-moesin homology (FERM) protein domain is a multifunctional protein-lipid binding site, constituting an integral part of numerous membrane-associated proteins. Its interaction with the lipid phosphatidylinositol-4,5-bisphosphate (PIP_2), located at the inner leaflet of eukaryotic plasma membranes, is important for localization, anchorage, and activation of FERM-containing proteins. FERM-PIP_2 complexes structurally determined so far exclusively feature a 1:1 binding stoichiometry of protein and lipid, with a few basic FERM residues neutralizing the −4 charge of the bound PIP_2. Whether this picture from static crystal structures also applies to the dynamic interaction of FERM domains on PIP_2 membranes is unknown. We here quantified the stoichiometry of FERM-PIP_2 binding in a lipid bilayer using atomistic molecular dynamics simulations and experiments on solid supported membranes for the FERM domains of focal adhesion kinase and ezrin. In contrast to the structural data, we find much higher average stoichiometries of FERM-PIP_2 binding, amounting to 1:3 or 1:4 ratios, respectively. In simulations, the full set of basic residues at the membrane interface, 7 and 15 residues for focal adhesion kinase and ezrin, respectively, engages in PIP_2 interactions. In addition, Na ions enter the FERM-membrane binding interface, compensating negative PIP_2 charges in case of high charge surpluses from bound PIP_2. We propose the multivalent binding of FERM domains to PIP_2 in lipid bilayers to significantly enhance the stability of FERM-membrane binding and to render the FERM-membrane linkage highly adjustable.

SIGNIFICANCE Four-point-one ezrin-radixin-moesin homology (FERM) domains are widespread modules that localize proteins to membranes by binding negatively charged phosphatidylinositol-4,5-bisphosphate (PIP_2) lipids. All current experimental PIP_2-FERM structures show one PIP_2 per FERM, but if this 1:1 stoichiometry holds at a dynamic FERM-membrane interface is unknown. Our atomistic simulations and biophysical experiments of two different FERM domains, those of focal adhesion kinase and ezrin, reveal that these FERM domains bind multiple PIP_2 molecules in a highly dynamic fashion. This highlights the importance of dynamic binding information in addition to static structures. Furthermore, we show how one principle, namely accumulation of basic residues on the FERM domain surface to recruit multiple PIP_2 molecules, apparently evolved independently at two distinct sites in the two model proteins studied.

INTRODUCTION

Located at the N-terminus of numerous peripheral membrane proteins, the band four-point-one ezrin-radixin-moesin homology (FERM) domain mediates the interaction with transmembrane proteins, signaling proteins, or lipids. It is involved in important signaling tasks and linking of the cortical actin cytoskeleton to the cytoplasmic leaflet of the plasma membrane (1). The FERM domain, as first discovered in the eponymous proteins ezrin, radixin, and moesin (ERM family), is composed of three subdomains (lobes), F1–F3, that arrange in the characteristic cloverleaf-shaped fold (Fig. 1).

A common feature shared by many FERM domains is their high-affinity interaction with the lipid phosphatidylinositol-4,5-bisphosphate (PIP_2), which is often necessary for successful targeting and anchorage of FERM-containing proteins to the plasma membrane (4) and has been shown to constitute an integral part of the activation mechanism of several FERM-containing proteins (3,5).

Submitted October 29, 2022, and accepted for publication February 18, 2023.

*Correspondence: csteine@gwdg.de or frauke.graeter@h-its.org

Editor: Lucie Delemotte.

https://doi.org/10.1016/j.bpj.2023.02.027

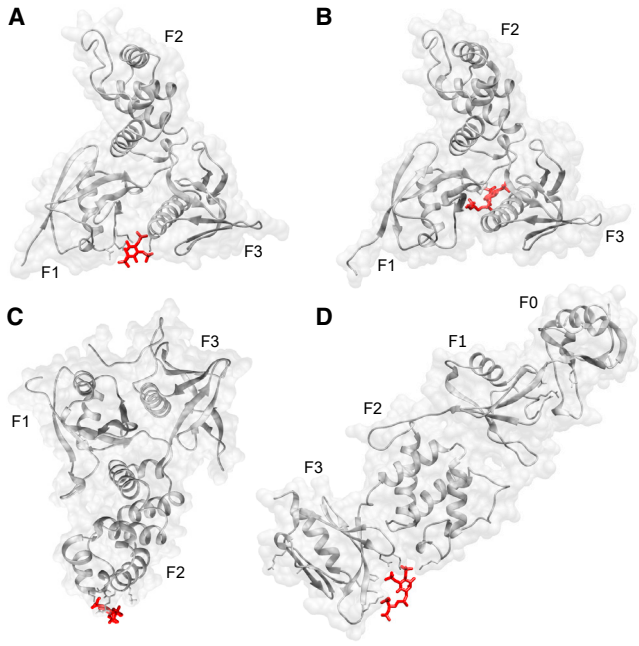

FIGURE 1 The FERM domains (*gray*) of different proteins interact with PIP_2 via different binding sites. (*A*) Radixin-FERM in complex with inositol-(1,4,5)-triphosphate, (*B*) merlin-FERM-PIO complex (PIO = PIP2diC8), (*C*) FAK-FERM domain, and (*D*) talin-FERM-PIO. The PDB accession codes are PDB: 1GC6, 6CDS, 6CB0 (2), and 6MFS, respectively. The PIP_2 analogs are depicted in red. The location of the PIP_2 molecule bound to the FAK-FERM domain in (*B*) goes back to a model of focal adhesion kinase used in a previous MD simulation study (3). To see this figure in color, go online.

Despite strong conservation of the FERM domain's clover-leaf-shaped fold, past research has shown that different members of the FERM superfamily interact with PIP_2 via distinct binding sites on the FERM domain, partly assuming different binding poses with respect to the plasma membrane. While most FERM-containing proteins, including the ERM family members, orient the F1 and F3 lobes of their FERM domains toward the plasma membrane, focal adhesion kinase (FAK) presents the F2 lobe of its FERM domain to the plasma membrane, i.e., assumes a reversed binding pose (Fig. 1 *C*).

At the time of preparing this article, there are three FERM domain crystal structures complexed with PIP_2 analogs deposited on in the PDB. These FERM domains stem from the proteins radixin, merlin, and talin1. On the basis of the radixin-FERM-PIP_2 complex (PDB: 1GC6), radixin was suggested to possess a PIP_2-binding site in the basic cleft between its F1 and F3 lobes (6) (Fig. 1 *A*), which, in view of the high sequence identity of $\sim 85\%$ among ERM family FERM domains (7) and mutagenesis studies (4), is thought to be present in ezrin and moesin as well. Despite the still high sequence identity of $\sim 60\%$ between the FERM domains of merlin and radixin (8), the merlin-FERM-PIP_2 complex (PDB: 6CDS) is observed to have a unique PIP_2-binding site between the F1 and F3 lobes located approximately 17 Å away from radixin's PIP_2-binding site (Fig. 1 *B*) (9). The cytoskeletal protein talin1 is an exceptional member of the FERM superfamily inasmuch as its FERM domain features a linear, rather than cloverleaf-shaped, arrangement, with an additional lobe F0 prepending the F1–F3 lobes. The talin1-FERM-PIP_2 complex (PDB: 6MFS) indicates yet another PIP_2-binding site between the F2 and F3 lobes (10) (Fig. 1 *D*).

Notably, all three abovementioned FERM-PIP_2 complexes are bound by a single PIP_2 analog at only one binding site, suggesting a stoichiometry of FERM-PIP_2 binding of 1:1.

Here, we performed molecular dynamics (MD) simulations and protein-binding studies of the FAK and ezrin FERM domains on phosphatidylcholine (POPC) lipid bilayers doped with PIP_2 to question the 1:1 stoichiometry observed in crystal structures. We chose these two FERM domain basic clefts as they differ in their position on the FERM domain as well as the local distribution of basic residues at the cleft (compare Fig. 1, *A* and *C*). We consistently identified higher numbers of PIP_2 bound to the proteins than the 1:1 ratio suggested by the crystal structures. We find the interaction surface of protein basic residues with the PIP_2 membrane to extend much beyond the known basic patch previously identified by crystallography or mutagenesis, thereby reaching out to rather $\sim$3–5 PIP_2 molecules at a time. Our joint experimental and simulation data reveal specific protein-PIP_2 interactions to be strongly multivalent and of surprisingly dynamic nature.

MATERIALS AND METHODS

Atomistic MD simulations

The starting structures for our MD simulations were modeled based on structures of the ezrin-FERM domain (PDB: 4RMA (11)) and the FAK-FERM domain (PDB: 6CB0 (2)). A structural fit of the ezrin-FERM domain to the sequentially and structurally very similar radixin-FERM domain of the FERM-PIP_2 complex in Fig. 1 *A* and repeated use of the functionalities provided by the CHARMM-GUI Membrane Builder (12,13) allowed us to obtain an ezrin-FERM-PIP_2 complex of reasonable orientation with respect to an underlying 9.1×9.1 nm lipid bilayer (details in supporting material). To assemble the FAK-FERM-membrane starting structure, we used a previously modeled FAK-dimer-PIP_2 complex (3), based on a cryoelectron microscopy structure of a FAK dimer that was subjected to a rigorous PIP_2 docking procedure, as a template. Structurally fitting the FAK-FERM structure to one of the two FAK-FERM domains contained in this template structure and again making use of the CHARMM-GUI Membrane Builder, we assembled a reasonably oriented FAK-FERM-membrane starting structure (details in supporting material). The underlying lipid bilayer had dimensions 9.5×9.5 nm. In both systems, the lipid bilayer was composed of POPC lipids with 10% PIP_2 in the protein-proximal leaflet. All MD simulations were performed with GROMACS (14) 2018.5 using the CHARMM36 (15) additive all-atom force-field (v.March 2019). The assembled ezrin- and FAK-FERM-membrane structures were placed in simulation boxes of sizes $9.2 \times 9.2 \times 15$ nm and $9.75 \times 9.75 \times 18$ nm, respectively, and solvated in TIP3P water (16). All simulations were performed in the presence of NaCl specifying a target concentration of 150 mM. In energy minimization, using steepest descent, the systems were steered toward nearby local minima of the potential energy until the maximal occurring force dropped below $F_{\mathrm{tol}} = 1000\ \frac{\mathrm{kJ}}{\mathrm{nm \cdot mol}}$. After initial

temperature and pressure adjustment to $T = 303$ K and $p = 1$ bar according to the CHARMM equilibration protocol (13), production runs were carried out in the NPT ensemble. To this end, temperature coupling was switched from velocity rescaling (17) to Nosé-Hoover coupling (18,19) with a coupling time constant of $\tau_{tc} = 1$ ps and semiisotropic pressure coupling switched from Berendsen (20) to Parrinello-Rahmann (21,22) coupling with a coupling time constant of $\tau_{pc} = 5$ ps and isothermal compressibility kept at $\kappa = 4.5 \times 10^{-5}$ bar^{-1}. Constraining bonds involving hydrogen with the LINCS algorithm (23), an integration time step of $\Delta t = 2$ fs could be used. Van der Waals forces were smoothly switched to zero between $r_{sw} = 1.0$ nm and $r_{vdw} = 1.2$ nm, and for both the evaluation of van der Waals interactions and the direct part of the Ewald sum, Verlet neighbor lists were used, which were updated every $n_{list} \geq 20$ integration steps. Evaluation of the reciprocal part of the Ewald sum was done with the smooth particle mesh Ewald technique at a Fourier grid spacing of 0.14 nm. For the ezrin- and FAK-FERM domains, a total of 8.1 and 6.9 μs of equilibrium simulation data were collected in 10 independent replicates, respectively. Additionally, for each FERM domain, six replicates were continued for a further 100 ns with higher write-out frequency of ion coordinates (details in supporting material).

Based on stabilization of FERM-PIP_2 contact maps computed with ConAn as an equilibration criterion, we discarded the first 600 ns of each ezrin-FERM simulation and the first 450 ns of each FAK-FERM simulation as equilibration time (details in supporting material).

Evaluation of FERM-PIP_2 stoichiometry

The histograms of the stoichiometry of FERM-PIP_2 binding (Fig. 2) were obtained by counting for each simulation frame of the equilibrated portion of the MD data the number of PIP_2 molecules bound to the respective FERM domain. A PIP_2 molecule was considered to be bound to a FERM domain if at least one of its phosphate groups got within 0.6 nm of the protonated end of a Lys or Arg residue (details in supporting material).

Contact analysis

To determine residue-wise FERM-PIP_2 contacts (Fig. 4, *E* and *F*) and the contributions of FERM-PIP_2 contacts to the overall FERM-membrane contacts (Table 1), ConAn was deployed, turning residue-lipid interactions on when interaction partners got within $d \leq d_{inter} = 0.4$ nm and off when they got separated by $d > d_{high} = 0.6$ nm (details in supporting material).

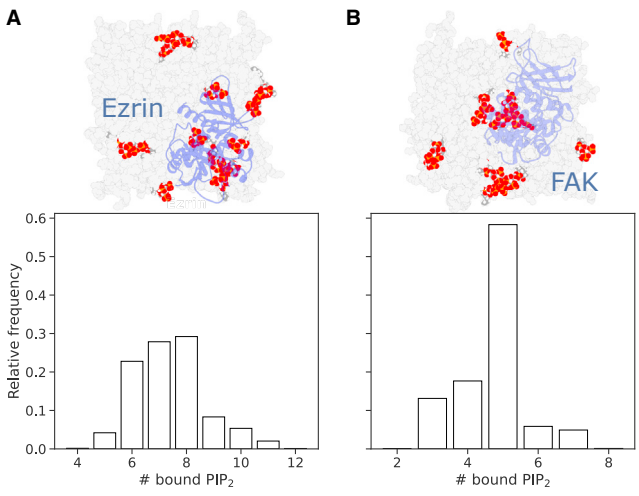

FIGURE 2 The stoichiometry of FERM-PIP_2 binding is larger than suggested by FERM-PIP_2 complexes deposited on the PDB. Normalized stoichiometry histograms computed on the basis of MD simulation data are shown for (*A*) the ezrin-FERM and (*B*) the FAK-FERM domain. The simulation snapshots above the histograms show the FERM domains (*blue*) in interaction with PIP_2 molecules (*red*). The underlying membrane is colored in light gray. To see this figure in color, go online.

Isolation of recombinant ezrin-FERM and FAK-FERM

Proteins were recombinantly expressed in *Escherichia coli* as previously described by Schäfer et al. for ezrin-FERM and Ceccarelli et al. for FAK-FERM (24,25). The protocol for ezrin-FERM purification was followed strictly. The protocol for the FAK-FERM was adjusted starting with the pET28a vector with the respective DNA sequence kindly provided by Daniel Lietha (Margaritas Salas Center for Biological Research, Madrid, Spain). After transformation of the vector in a BL21(De3)pLysS strain (Novagen, Madison, WI, USA), the cells were grown to an OD_{600} of 0.8, and protein expression was induced by the addition of 0.2 mM IPTG and incubated for 12–16 h at 18°C. The cells were pelleted and lysed in buffer A (20 mM Tris [pH 8], 10 mM β-mercaptoethanol, and 5 mM imidazole) with 200 mM NaCl and additionally containing an inhibitor cocktail tablet (cOmplete; Roche Diagnostics, Basel, Switzerland). The cells were sonicated and centrifuged for 1 h at 100,000 $\times$ *g*. Afterward, the supernatant was loaded on a Ni-NTA column and eluted with buffer A containing 200 mM NaCl and 195 mM imidazole additionally. The His tag of the protein was cleaved off from the pooled fractions by a TEV protease (Merck KGaA, Darmstadt, Germany) using a ratio of 1:100 (*w/w*) at 4°C during dialysis to buffer A with 50 mM NaCl. The protein was loaded on a Mono Q 5/50 GL column (Merck KGaA, Darmstadt, Germany) and eluted with a buffer A gradient from 50 mM NaCl to 1 M NaCl. The fractions containing the FAK were combined and loaded onto a HiLoad 16/600 Superdex column (Merck KGaA, Darmstadt, Germany) equilibrated with buffer A containing 150 mM NaCl. The eluted protein was concentrated and stored at 4°C.

Reflectometric interference spectroscopy (RIfS)

RIfS experiments were performed using a custom-build instrument with a Flame-S-UV-visible spectrometer (OceanOptics Germany GmbH, Ostfildern, Germany). With the setup, the optical thickness of a thin layer on a SiO_2 wafer can be determined by the reflection of white light, which was measured every 2 s (26). Si substrates with a 5 μm oxide layer were cleaned with an $H_2O/NH_3/H_2O_2$ (5:1:1) solution at 70°C for 20 min. The cleaned wafers were treated with an O_2 plasma for 30 s and used directly afterward. After obtaining a baseline with Na-citrate buffer (50 mM NaCl, 20 mM Na-citrate, 0.1 mM EDTA, 0.1 mM NaN_3 [pH 4.8]), small unilamellar vesicles were added to form a supported lipid bilayer. Small unilamellar vesicles were obtained by sonication of a lipid mixture of POPC and PIP_2 (Avanti Polar lipids, Alabaster, AL, USA) in Na-citrate buffer with different POPC:PIP_2 ratios (99:1–90:10). The quality of the supported lipid bilayers was proven by the ΔOT values after spreading. After a buffer exchange to buffer A with 150 mM NaCl for 10 min, a thoroughly mixed protein solution was added. FAK-FERM was added with a final concentration of 800 μM, whereas ezrin-FERM was added with a final concentration of 70 μM. The different concentrations take the different binding affinities into account, ensuring that all available PIP_2-binding sites are occupied. The

TABLE 1 Contribution of PIP_2 to overall FERM-membrane contacts

	Ezrin-FERM	FAK-FERM
FERM-membrane	64 ± 5	20 ± 2
FERM-PIP_2	23 ± 3	9.4 ± 1.3

Average and standard error of the mean of contacts between FERM domain residues and all membrane lipids or only PIP_2 lipids are shown.

obtained data were evaluated using a self-written MATLAB script (The MathWorks, Natick, MA, USA).

RESULTS

Stoichiometry of FERM-PIP_2 binding is larger than expected

We determined the stoichiometries of FERM-PIP_2 binding of the ezrin- and FAK-FERM domains through MD simulations and stoichiometry experiments on lipid bilayers composed of POPC and PIP_2. By counting the number of PIP_2 molecules bound to the FERM domains for each simulation frame of the equilibrated portions of the MD trajectories, normalized histograms of stoichiometry were computed (Fig. 2).

For both FERM domains, the probability of binding PIP_2 increases up to an ideal range of bound PIP_2 molecules, above which probability drops markedly and decays to zero. While the ezrin-FERM domain is most likely bound by 6–8 PIP_2 molecules with an average binding count of $\overline{N}_{PIP2,ezrin} = 7.4 \pm 0.4$ (standard error of the mean), the FAK-FERM domain is most often bound by 5 PIP_2 molecules with an average binding count of $\overline{N}_{PIP2,FAK} = 4.6 \pm 0.3$ (standard error of the mean).

To investigate experimentally whether the hypothesis that both FERM domains bind more than one PIP_2 molecule as derived from our MD simulations, we analyzed the binding of FAK-FERM and ezrin-FERM to POPC lipid bilayers on Si substrates doped with different PIP_2 concentrations. By means of RIfS, we determined the change in optical thickness (ΔOT) upon protein binding to the supported lipid bilayer dependent on the PIP_2 concentration (Fig. 3, *A* and *B*). ΔOT is a measure of the protein surface coverage. High protein concentrations were chosen to assume that all PIP_2 molecules are occupied by protein. The Hill equation (Eq. 1) was fitted to the sigmoidal change of ΔOT as a function of the total PIP_2 surface concentration $\Gamma_{PIP2,0}$:

$$\Delta OT = \Delta OT_{max} \frac{\Gamma^n_{PIP2,0}}{K_D + \Gamma^n_{PIP2,0}} \qquad \text{(Equation 1)}$$

For the FAK-FERM, a $\Delta OT_{FAK-FERM(max)} = 4.5$ nm was determined with $n_{FAK-FERM} = 3.6$. For the ezrin-FERM, $n_{ezrin-FERM} = 5.5$ and $\Delta OT_{ezrin-FERM(max)} = 3.6$ nm were found. $\Delta OT_{FAK-FERM(max)}$ is defined as $n_{protein} \times d_{FAK-FERM}$, with $n_{protein} = 1.455$ being the refractive index of the protein layer (27). That means that an average physical protein layer thickness of $d_{FAK-FERM} = 3$ nm can be calculated for the FAK-FERM, whereas for ezrin-FERM, $d_{ezrin-FERM}$ would read 2.5 nm. Based on the ΔOT_{max} values, we defined the surface coverage $\Theta_{protein} = \Delta OT/\Delta OT_{max} = 1$. The exponent n in Eq. 1 refers to the cooperativity of binding and is often interpreted as the number of bound ligands. However, even though the Hill equation fits the data nicely, the assumption of a cooperative binding of ligands to a protein in three dimensions is not valid in a two-dimensional membrane system. To arrive at an equation (Eq. 2) that takes into account that only protein binding to the PIP_2-doped membrane surface can be measured by RIfS and where no direct information about the number of PIP_2 molecules per protein can be obtained, we defined multiple binding reactions at the membrane similar to the work of Mosior and co-workers (supporting material) (28,29):

$$\Theta_{protein} = A_p N_A (\Gamma_{PIP2,0} - \Gamma_{PIP2}) \frac{\sum_{i=1}^{n} (K_S \Gamma_{PIP2})^{i-1}}{\sum_{i=1}^{n} i (K_S \Gamma_{PIP2})^{i-1}} \qquad \text{(Equation 2)}$$

A_p is the footprint of the protein, N_A the Avogadro constant, Γ_{PIP2} the free PIP_2 surface concentration, n the number of PIP_2 molecules bound to the protein and K_S the surface binding constant. We have taken the molecular protein area and the surface molecular coverage to calculate $A_p = A_{one}/\alpha$ from the MD simulations leading to $\Theta_{protein} = 1$. K_S was calculated from the Gibbs free energies of binding (MD simulations; see supporting material) and the assumption that the surface is treated as a region of finite thickness with $h = 10$ nm (28,29). The system is still underdetermined, and the free PIP_2 surface concentration cannot be determined independently. Thus, we calculated Γ_{PIP2} ($\Gamma_{PIP2,0}$) plots for different n and found that Γ_{PIP2} becomes negative if n exceeds a certain value. We define this n as being the maximum PIP_2 molecules bound to the protein (supporting material). Using this approach, $n < 3$ was determined for the FAK-FERM,

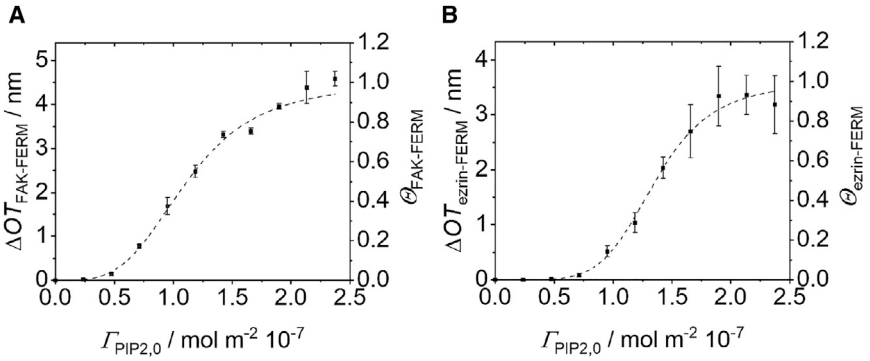

FIGURE 3 Binding of FAK-FERM (*A*) and ezrin-FERM (*B*) on PIP_2-doped membranes. Change of the optical thickness (ΔOT) upon binding of FAK-FERM (800 μM) or ezrin-FERM (70 μM) on POPC/PIP_2 SLBs with varying PIP_2 surface concentrations. Error bars indicate the standard error of the mean ($N \geq 4$). Eq. 1 was fit to the data (*dashed lines*), resulting in $\Delta OT_{FAK-FERM(max)} = 4.5$ nm with $n_{FAK-FERM} = 3.6$ and $\Delta OT_{ezrin-FERM(max)} = 3.6$ nm with $n_{ezrin-FERM} = 5.5$. $\Theta_{protein} = \Delta OT/\Delta OT_{max}$. To see this figure in color, go online.

whereas for the ezrin-FERM, $n < 4$. The reduced n values compared with those obtained by fitting a Hill equation to the data are in agreement with the idea that the dimensionality is reduced upon the first binding of the protein to the quasi two-dimensional membrane (28,29).

Lateral PIP_2 distribution follows distribution of positive residues on the FERM domain surface

With average binding stoichiometries of five or even seven PIP_2 molecules per FERM domain in the simulations, it is not immediately clear where on the FERM domain surfaces all of these PIP_2 molecules could be accommodated. To get a first overview of the sites of FERM-PIP_2 interaction, we visualized the interaction surfaces of the ezrin- and FAK-FERM domains by plotting the lateral PIP_2 distribution around the two different FERM domains (Fig. 4, *A* and *B*).

For both FERM domains, lateral PIP_2 distribution closely follows the charge distribution generated by the Lys and Arg residues on the FERM domain surfaces of ezrin and FAK. The patch-like positively charged interaction surface (Fig. 4 *B*) the FAK-FERM domain's F2 lobe offers the PIP_2 molecules for interaction is in stark contrast to the widespread charge distribution on the interaction surface of the ezrin-FERM domain (Fig. 4 *A*).

To quantitatively pin down the main sites of FERM-PIP_2 interaction, we computed the average total contacts formed by individual protein residues with PIP_2 molecules using the contact analysis tool ConAn (30) (Fig. 4, *E* and *F*).

The residue-wise average total contacts first of all indicate that it is indeed primarily Lys and Arg residues that frequently interact with PIP_2. As expected, the residues comprising the crystallographic binding site in the basic cleft between the F1 and F3 lobes of the ezrin-FERM domain (K60, K63, K83, K278, and R279) and the basic patch on the F2 lobe of the FAK-FERM domain (K216, K218, R221, and K222) are in pronounced interaction with PIP_2 molecules. Interestingly, however, the residue-wise contact analysis also reveals many other residues on the FERM domain surfaces that interact with PIP_2 at a comparable frequency. Whereas the ezrin-FERM residues K53 (F1 lobe) and R273 and R275 (F3 lobe) are found in close proximity to the basic cleft and thus effectively extend it, other strongly interacting residues like R246, K253, K254, K258, K262, and K263 are spread over the outer loops of the F3 lobe (Fig. 4 *C*). Noting also K3 and the less strongly interacting residues K35, K40, and K72 on the F1 lobe, as well as the residues R293 and K296 on the opposite side of a long α-helix of the F3 lobe, one realizes that positive residues are scattered all over the outer F1 and F3 lobes of the ezrin-FERM domain, thus maximizing its interaction surface. With R184, K190, and K191 on a neighboring α-helix of the F2 lobe, the FAK-FERM domain has three more strongly interacting protein residues beside the more prominent basic patch residues (Fig. 4 *D*) (3,31).

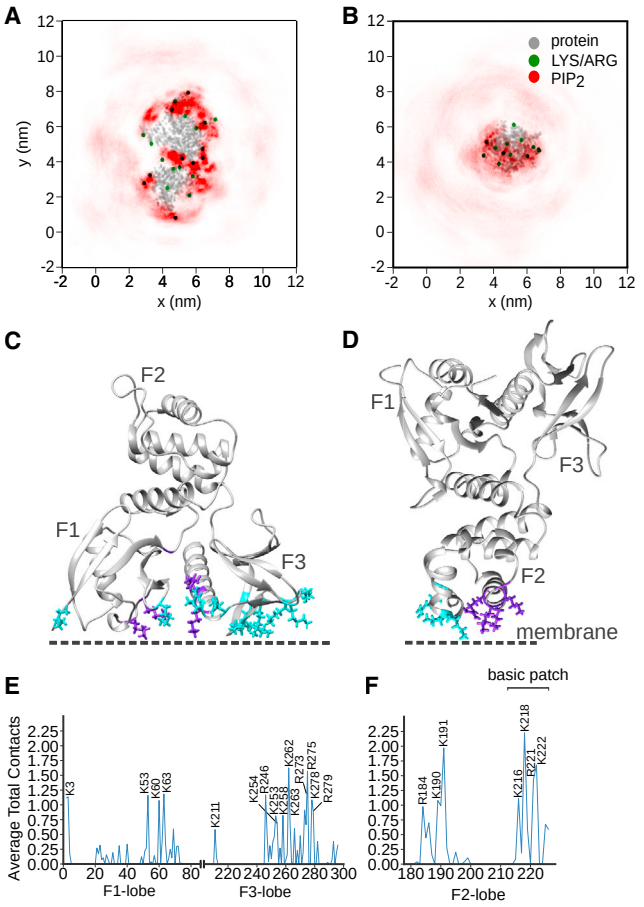

FIGURE 4 The FERM domains of ezrin and FAK interact with PIP_2 via several different binding sites. (*A* and *B*) Lateral distribution of PIP_2 (*red*) around the ezrin- and FAK-FERM domains (*gray*). Green dots represent the protonated ends of Lys or Arg residues. The visualizations are based on simulation frames subjected to rotational and translational fits to a common reference structure (details in supporting information). (*C* and *D*) Sites of FERM-PIP_2 interaction on the ezrin- and FAK-FERM domains. The crystallographic basic cleft (ezrin) and basic patch (FAK) residues are colored purple. Additional, frequently interacting Lys and Arg are depicted in cyan. (*E* and *F*) Average total contacts per frame of ezrin-/FAK-FERM residues with PIP_2 molecules. We counted contacts when the minimal distance between a protein residue and PIP_2 was below 0.6 nm, summed the number of contacts of each residue, and averaged over the whole simulation time. Lys and Arg with $\overline{n}_{res} \geq 0.5$ average total contacts per frame were labeled in single letter amino acid code. To see this figure in color, go online.

FERM-PIP_2 contacts contribute strongly to overall FERM-membrane contacts

Finding a large number of positively charged FERM residues in pronounced interaction with PIP_2, we became interested in the contribution of FERM-PIP_2 interactions to FERM-membrane binding strength. We therefore compared the number of contacts of protein residues with all membrane lipids and with only PIP_2 lipids (Table 1).

Since the PIP_2 content in the protein-proximal membrane leaflet is 10%, we would expect that FERM-PIP_2 contacts account for 10% of the overall FERM-membrane contacts

assuming an even distribution of PIP_2 lipids across the membrane as initially constructed. However, FERM-PIP_2 contacts contribute 36% and 47% of the overall ezrin-FERM- and FAK-FERM-membrane contacts, respectively. We conclude that PIP_2 accumulates below the proteins, while the unoccupied membrane regions consequentially possess a lower PIP_2 content.

DISCUSSION

Here, we probed the stoichiometry of FERM-PIP_2 interaction of the proteins ezrin and FAK in atomistic MD simulations and in experiments on SLBs. Both simulations of single FERM domains on a PIP_2-containing lipid bilayer and stoichiometry experiments involving layers of typically oligomerized FERM domains suggest that the stoichiometry of FERM-PIP_2 binding is much larger than expected on the basis of the three FERM-PIP_2 complexes deposited on the PDB (PDB: 1GC6, 6MFS, and 6CDS). Our experimental data point at a stoichiometry of ~3–4 PIP_2 molecules per FERM domain for FAK and ezrin, respectively.

To estimate the stoichiometry of FERM-PIP_2 binding experimentally, we analyzed the data first using a well-known Hill equation. The Hill equation describes protein-ligand binding and allows accessing the degree of cooperativity of reactions that occur in three dimensions, with the assumptions that the n binding sites are independent and identical (28). However, any reaction occurring at the membrane interface is subdivided into a first reaction taking place from solution but is then confined in the plane of the membrane, i.e., becomes two-dimensional. This reduction in dimensionality overestimates the stoichiometry given by the Hill coefficient n (28).

Thus, we applied a model following the assumption of Mosior and McLaughlin (28,29). The three-dimensional region, where the protein first binds to a ligand in the membrane is treated as a region of finite thickness of 10 nm. As the protein-ligand interaction at the membrane interface itself cannot be resolved by the measurement, the resulting set of equations is underdetermined. To still obtain a lower estimate of the number of ligands (PIP_2 molecules) bound to one protein, we defined the number of PIP_2 molecules, where $\Gamma_{PIP2} = 0$ applies. If n is an integer, n is defined where Γ_{PIP2} , 0, defining the minimum number of bound PIP_2 molecules per FERM domain. The obtained n values derived from this model are for both proteins around one lower ($n < 3$ for FAK-FERM and $n < 4$ for ezrin-FERM) than the n values obtained from fitting the Hill equation to the data ($n = 3.6$ for FAK-FERM and $n = 5.5$ for ezrin-FERM) (Fig. 3, *A* and *B*). This is in agreement with our expectation that the Hill equation overestimates the number of bound ligands in a two-dimensional system.

In our simulations, we found even larger stoichiometries of 5 and 6–8 PIP_2 molecules per FERM domain for FAK and ezrin, respectively. These values are consistent with previous simulations. The ezrin-FERM domain's stoichiometry reported here falls within a similar range as the PIP_2 binding count of 6 ± 0.3 previously observed in atomistic MD simulations of the closely related protein moesin on a lipid bilayer with the composition POPC:POPE:POPS:PIP_2 50:20:20:10 (mol/mol) (32). We note that our chosen cutoff for defining bound PIP_2 molecules, albeit being based on the Bjerrum length, is arbitrary. Additionally, the larger stoichiometry in simulations compared with experimental data could be explained by the finding that MD force-fields commonly overstabilize salt bridges (33). A previous attempt to avoid the overstabilization of salt bridges using the Amber99SB* ILDN-DERK force-field, which applies adjusted charges for Glu, Asp, Arg, and Lys residues, has not improved this problem (34). Overall, both experiments and simulations agree that the stoichiometries for both proteins of binding PIP_2 are much larger than one and suggest a larger number of bound PIP_2 molecules for ezrin's FERM domain with a larger, more diffuse basic interaction area compared with FAK.

The large stoichiometry of FERM-PIP_2 binding implies that the positive charges of the basic residues at the membrane surface are roughly compensated, if not overcompensated, by negative charges of PIP_2s. Experiments suggest ~4 PIP_2s or charge $\sim -16\,e$ for 15 Lys/Arg of ezrin and ~3 PIP_2s or charge $\sim -12\,e$ for 7 Lys/Arg of FAK, considering the experimentally determined (35) PIP_2 net charge at pH 7 of $\sim -4\,e$ per molecule. PIP_2 counts in our simulations translate to a charge of $\sim -30\,e$ and $\sim -18\,e$ for ezrin and FAK, respectively. At the same time, we observe a standard deviation of approximately ~1 PIP_2, or a charge of $\sim -4\,e$, for the average number of bound PIP_2s in our MD simulations. As a consequence, negative charges dynamically vary and can exceed the positive protein charges at the interface. In such cases, our simulations predict that Na ions, being only partially displaced upon binding of PIP_2 to the protein, enter the binding interface, where they can neutralize a negative net charge of the protein-membrane interface (Figures S4–S6). However, this raises the question of why PIP_2 prefers to interact with the protein if Na ions could, in principle, compensate its charge. When we compared the charges of free and bound PIP_2 clusters, we found that Na ions and PIP_2 interact at a 3:1 ratio, leaving an excess charge of $\sim -1\,e$ for each PIP_2 molecule per cluster. This charge is neutralized by the positively charged protein residues, electrostatically biasing PIP_2 toward the protein interface, which also explains the large contribution of PIP_2 lipids to the overall FERM-membrane contacts (Table 1). We note that this simple consideration is based on charge summation and neglects the spatial distribution of charges or any less-simple contributions to the system's free energy, which can further modify the stoichiometries. Also, our computational analysis is based on orientations of the FERM domains, as suggested by cocrystals with PIP2, while other orientations cannot be excluded and can

only be partially covered by rocking motions within our submicrosecond simulations (Fig. S3).

Seeking to understand where on the ezrin- and FAK-FERM domains more than one PIP_2 molecule could be accommodated, we mapped out the FERM's main PIP_2 interaction sites and visualized the interaction surfaces (Fig. 4). As expected in view of PIP_2's substantial negative net charge, it was primarily the positively charged Lys and Arg that interacted frequently with PIP_2. Moreover, we observed lateral PIP_2 distribution to closely follow the distribution of positive charge determined by the Lys and Arg on the FERM domain surfaces. This type of visualization underlined the rather small patch-like interaction surface presented by the FAK-FERM domain to the membrane and showed that almost the entire surface of the ezrin-FERM domain is involved in the interaction. Residue-wise contact analysis further revealed that PIP_2 molecules interact frequently with many other Lys and Arg besides the well-established residues comprising the binding site in the basic cleft of the ezrin-FERM domain or the basic patch of the FAK-FERM domain.

Also taking into account less frequently interacting residues on the F1 and F3 lobes, our results are in keeping with the list of interacting residues reported in the above-mentioned MD simulations of moesin (32). It is interesting to note that despite the FERM domains' conserved fold, PIP_2-binding sites have apparently evolved at different positions. Yet, stable FERM-membrane binding relies on the same principle, namely a cluster of basic residues interacting electrostatically with PIP_2 lipids and, at least in simulations, charge neutralization by Na ions. When comparing the FERM domain with pleckstrin homology (PH) domains, which are another family of lipid recognition domains, one discovers that the FERM F3 lobe shares the same fold as PH domains. PH domains also rely on electrostatic interactions between positively charged residues and the phosphatidylinositol phosphate PIP_3. In contrast to FERM domains, a conserved canonical PIP_3-binding site could be defined for PH domains (36). However, a noncanonical site and further residues were also found to be important for thermodynamically stable membrane interactions in coarse-grained MD simulations of the GRP1 PH domain (37), which is in line with our finding that residues additional to the well-characterized FAK basic patch and ezrin basic cleft contribute to FERM domain PIP_2 binding.

From a biological perspective, the exhaustive use of the ezrin-FERM surface for interaction with PIP_2 conforms well with ezrin's task to establish a robust link between the actin cortex and the plasma membrane. The usage of a smaller number of positive residues being concentrated on two neighboring α-helices on the F2 lobe might allow for a stable enough, but still readily detachable, membrane linkage, as required for a signaling enzyme like FAK. Membrane binding is required for autoactivation (38) and has to be strong enough to withstand the forces required for force activation (39,40). On the other hand, FAK has to be released from focal adhesions (FAs) for FA turnover. Therefore, carefully balanced thermodynamic and mechanical stability of membrane binding is crucial for normal cellular function. Stoichiometries of FERM-PIP_2 binding significantly beyond 1:1 render the protein-membrane interaction not only more stable but also adjustable. The PIP_2 concentration in the cytoplasmic leaflet of the plasma membrane depends on the activity of several enzymes, including, for example, the phosphatidylinositol phosphate kinase type Iγ, which synthesizes PIP_2 in FAs (41). Furthermore, we speculate that the ionic strength of the cytosol, importantly also the concentration of divalent ions, can regulate the strength of electrostatic FERM-PIP_2 binding.

In conclusion, our study quantifies and rationalizes the stoichiometry of the FERM-PIP_2 interaction of ezrin and FAK based on experiments and MD simulations performed on PIP_2-containing model membranes. The proposed rather large stoichiometry of FERM-PIP_2 binding ultimately entails a large contribution of the FERM-PIP_2 interaction to the overall FERM-membrane binding stability, which in turn results in a pronounced dependence of FERM-membrane interaction on local PIP_2 concentration. Our results underline the role of the FERM-PIP_2 interaction in controlling the activity of FERM-containing proteins. The mechanistic principles underlying the FERM-PIP_2 interaction uncovered here aid our understanding of the regulatory role of these proteins in cell adhesion, growth, and motility.

SUPPORTING MATERIAL

Supporting material can be found online at https://doi.org/10.1016/j.bpj.2023.02.027.

AUTHOR CONTRIBUTIONS

T.E., T.H., and S.d.B. designed and performed the research, analyzed the data, and wrote the manuscript. C.A.-S. performed research and analyzed data. F.G. and C.S. designed the research and wrote the manuscript.

ACKNOWLEDGMENTS

F.G. and S.d.B. acknowledge funding through the Deutsche Forschungsgemeinschaft (DFG, German Research Foundation) under Germany's Excellence Strategy – 2082/1 – 390761711. T.H. and C.S. thank the Max Planck School Matter to Life, and C.S. further acknowledges the DFG (STE 884/17-1) for funding. Moreover, F.G., C.A.-S., T.E., and S.d.B. acknowledge funding from the Klaus Tschira Foundation and the state of Baden-Württemberg through bwHPC, as well as the DFG through grant INST 35/1134-1 FUGG. S.d.B. thanks the Carl Zeiss Foundation for financial support. C.S. thanks A. Janshoff for fruitful discussions on the theoretical treatment of multivalent protein binding.

DECLARATION OF INTERESTS

The authors declare no competing interests.

SUPPORTING CITATIONS

References (2,3,6,11–13,30,35,42–49) appear in the supporting material.

REFERENCES

1. Bretscher, A., K. Edwards, and R. G. Fehon. 2002. ERM proteins and merlin: integrators at the cell cortex. *Nat. Rev. Mol. Cell Biol.* 3:586–599.
2. Marlowe, T., A. Dementiev, …, W. Cance. 2019. High resolution crystal structure of the FAK FERM domain reveals new insights on the Druggability of tyrosine 397 and the Src SH3 binding site. *BMC Mol. Cell Biol.* 20:10.
3. Goñi, G. M., C. Epifano, …, D. Lietha. 2014. Phosphatidylinositol 4, 5-bisphosphate triggers activation of focal adhesion kinase by inducing clustering and conformational changes. *Proc. Natl. Acad. Sci. USA.* 111:E3177–E3186.
4. Barret, C., C. Roy, …, P. Mangeat, V. Niggli. 2000. Mutagenesis of the phosphatidylinositol 4, 5-bisphosphate (PIP2) binding site in the NH2-terminal domain of ezrin correlates with its altered cellular distribution. *J. Cell Biol.* 151:1067–1080.
5. Shabardina, V., C. Kramer, …, C. Steinem. 2016. Mode of ezrin-membrane interaction as a function of PIP2 binding and pseudophosphorylation. *Biophys. J.* 110:2710–2719.
6. Hamada, K., T. Shimizu, …, T. Hakoshima. 2000. Structural basis of the membrane-targeting and unmasking mechanisms of the radixin FERM domain. *EMBO J.* 19:4449–4462.
7. Martin, T. A., G. Harrison, …, W. G. Jiang. 2003. The role of the CD44/ezrin complex in cancer metastasis. *Crit. Rev. Oncol. Hematol.* 46:165–186.
8. Pearson, M. A., D. Reczek, …, P. A. Karplus. 2000. Structure of the ERM protein moesin reveals the FERM domain fold masked by an extended actin binding tail domain. *Cell.* 101:259–270.
9. Chinthalapudi, K., V. Mandati, …, T. Izard. 2018. Lipid binding promotes the open conformation and tumor-suppressive activity of neurofibromin 2. *Nat. Commun.* 9:1338.
10. Chinthalapudi, K., E. S. Rangarajan, and T. Izard. 2018. The interaction of talin with the cell membrane is essential for integrin activation and focal adhesion formation. *Proc. Natl. Acad. Sci. USA.* 115:10339–10344.
11. Phang, J. M., S. J. Harrop, …, P. M. G. Curmi. 2016. Structural characterization suggests models for monomeric and dimeric forms of full-length ezrin. *Biochem. J.* 473:2763–2782.
12. Jo, S., T. Kim, V. G. Iyer, and W. Im. 2008. CHARMM-GUI: a web-based graphical user interface for CHARMM. *J. Comput. Chem.* 29:1859–1865.
13. Lee, J., X. Cheng, J. M. Swails, …, W. Im. 2016. CHARMM-GUI input generator for NAMD, GROMACS, AMBER, OpenMM, and CHARMM/OpenMM simulations using the CHARMM36 additive force field. *J. Chem. Theory Comput.* 12:405–413.
14. Van Der Spoel, D., E. Lindahl, …, H. J. C. Berendsen. 2005. GROMACS: fast, flexible, and free. *J. Comput. Chem.* 26:1701–1718.
15. Vanommeslaeghe, K., E. Hatcher, …, A. D. Mackerell, Jr. 2010. CHARMM general force field: a force field for drug-like molecules compatible with the CHARMM all-atom additive biological force fields. *J. Comput. Chem.* 31:671–690.
16. Jorgensen, W. L., J. Chandrasekhar, …, M. L. Klein. 1983. Comparison of simple potential functions for simulating liquid water. *J. Chem. Phys.* 79:926–935.
17. Bussi, G., D. Donadio, and M. Parrinello. 2007. Canonical sampling through velocity rescaling. *J. Chem. Phys.* 126:014101.
18. Hoover, W. G. 1985. Canonical dynamics: equilibrium phase-space distributions. *Phys. Rev. A Gen. Phys.* 31:1695–1697.
19. Nosé, S. 1984. A molecular dynamics method for simulations in the canonical ensemble. *Mol. Phys.* 52:255–268.
20. Berendsen, H. J. C., J. P. M. Postma, …, J. R. Haak. 1984. Molecular dynamics with coupling to an external bath. *J. Chem. Phys.* 81:3684–3690.
21. Nosé, S., and M. Klein. 1983. Constant pressure molecular dynamics for molecular systems. *Mol. Phys.* 50:1055–1076.
22. Parrinello, M., and A. Rahman. 1981. Polymorphic transitions in single crystals: a new molecular dynamics method. *J. Appl. Phys.* 52:7182–7190.
23. Hess, B., H. Bekker, …, J. G. E. M. Fraaije. 1997. LINCS: a linear constraint solver for molecular simulations. *J. Comput. Chem.* 18:1463–1472.
24. Schäfer, J., J. Nehls, …, C. Steinem. 2020. Leaflet-dependent distribution of PtdIns4,5P2 in supported model membranes. *Langmuir.* 36:1320–1328.
25. Ceccarelli, D. F. J., H. K. Song, …, M. J. Eck. 2006. Crystal structure of the FERM domain of focal adhesion kinase. *J. Biol. Chem.* 281:252–259.
26. Stephan, M., C. Kramer, …, A. Janshoff. 2014. Binding assay for low molecular weight analytes based on reflectometry of absorbing molecules in porous substrates. *Analyst.* 139:1987–1992.
27. Vörös, J. 2004. The density and refractive index of adsorbing protein layers. *Biophys. J.* 87:553–561.
28. Mosior, M., and S. McLaughlin. 1992. Electrostatics and reduction of dimensionality produce apparent cooperativity when basic peptides bind to acidic lipids in membranes. *Biochim. Biophys. Acta.* 1105:185–187.
29. Mosior, M., and A. C. Newton. 1998. Mechanism of the apparent cooperativity in the interaction of protein kinase C with phosphatidylserine. *Biochemistry.* 37:17271–17279.
30. Mercadante, D., F. Gräter, and C. Daday. 2018. CONAN: a tool to decode dynamical information from molecular interaction maps. *Biophys. J.* 114:1267–1273.
31. Cai, X., D. Lietha, …, M. D. Schaller. 2008. Spatial and temporal regulation of focal adhesion kinase activity in living cells. *Mol. Cell Biol.* 28:201–214.
32. Senju, Y., M. Kalimeri, …, P. Lappalainen. 2017. Mechanistic principles underlying regulation of the actin cytoskeleton by phosphoinositides. *Proc. Natl. Acad. Sci. USA.* 114:E8977–E8986.
33. Ahmed, M. C., E. Papaleo, and K. Lindorff-Larsen. 2018. How well do force fields capture the strength of salt bridges in proteins? *PeerJ.* 6:e4967.
34. Jin, F., and F. Gräter. 2021. How multisite phosphorylation impacts the conformations of intrinsically disordered proteins. *PLoS Comput. Biol.* 17:e1008939.
35. Kooijman, E. E., K. E. King, M. Gangoda, and A. Gericke. 2009. Ionization properties of phosphatidylinositol polyphosphates in mixed model membranes. *Biochemistry.* 48:9360–9371.
36. Ferguson, K. M., J. M. Kavran, …, M. A. Lemmon. 2000. Structural basis for discrimination of 3-phosphoinositides by pleckstrin homology domains. *Mol. Cell.* 6:373–384.
37. Yamamoto, E., J. Domański, …, M. S. P. Sansom. 2020. Multiple lipid binding sites determine the affinity of PH domains for phosphoinositide-containing membranes. *Sci. Adv.* 6:eaay5736.
38. Acebrón, I., R. D. Righetto, …, D. Lietha. 2020. Structural basis of Focal Adhesion Kinase activation on lipid membranes. *EMBO J.* 39:e104743.
39. Zhou, J., C. Aponte-Santamaría, …, F. Gräter. 2015. Mechanism of focal adhesion kinase mechanosensing. *PLoS Comput. Biol.* 11:e1004593.
40. Bauer, M. S., F. Baumann, …, D. Lietha. 2019. Structural and mechanistic insights into mechanoactivation of focal adhesion kinase. *Proc. Natl. Acad. Sci. USA.* 116:6766–6774.
41. Wu, Z., X. Li, M. Sunkara, H. Spearman, A. J. Morris, and C. Huang. 2011. PIPKIγ regulates focal adhesion dynamics and colon cancer cell invasion. *PLoS One.* 6:e24775.

42. Pettersen, E. F., T. D. Goddard, …, T. E. Ferrin. 2004. UCSF Chimera—a visualization system for exploratory research and analysis. *J. Comput. Chem.* 25:1605–1612.

43. Humphrey, W., A. Dalke, and K. Schulten. 1996. VMD: visual molecular dynamics. *J. Mol. Graph.* 14:33–38, 27-28.

44. Madeira, F., Y. M. Park, …, R. Lopez. 2019. The EMBL-EBI search and sequence analysis tools APIs in 2019. *Nucleic Acids Res.* 47:W636–W641.

45. Abraham, M., D. Van Der Spoel, …, B. Hess. 2014. GROMACS User Manual Version 5.0. 4. Royal Institute of Technology and Uppsala University.

46. Han, K., A. Gericke, and R. W. Pastor. 2020. Characterization of specific ion effects on PI (4, 5) P2 clustering: molecular dynamics simulations and graph-theoretic analysis. *J. Phys. Chem. B.* 124:1183–1196.

47. Lemkul, J. A., and D. R. Bevan. 2010. Assessing the stability of Alzheimer's Amyloid protofibrils using molecular dynamics. *J. Phys. Chem. B.* 114:1652–1660.

48. Hub, J. S., B. L. de Groot, and D. Van Der Spoel. 2010. g_wham— - a free weighted histogram analysis implementation including robust error and autocorrelation estimates. *J. Chem. Theory Comput.* 6:3713–3720.

49. Briones, R., C. Blau, C. Kutzner, B. L. de Groot, and C. Aponte-Santamaría. 2019. GROmaps: a GROMACS-based toolset to analyze density maps derived from molecular dynamics simulations. *Biophys. J.* 116:4–11.

Biophysical Journal, Volume *122*

Supplemental information

FERM domains recruit ample PI(4,5)P_2s to form extensive protein-membrane attachments

Thomas Ehret, Tim Heißenberg, Svenja de Buhr, Camilo Aponte-Santamaría, Claudia Steinem, and Frauke Gräter

Supporting Information - FERM domains recruit ample PI(4,5)P_2s to form extensive protein-membrane attachments

Thomas Ehret,[†] Tim Heißenberg,[‡] Svenja de Buhr,[†] Camilo Aponte-Santamaría,[†] Claudia Steinem,[*,‡,¶] and Frauke Gräter[*,§,†,¶]

†*Heidelberg Institute for Theoretical Studies (HITS), Heidelberg*

‡*Institute of Organic and Biomolecular Chemistry, University of Göttingen, Göttingen*

¶*Max Planck School Matter to Life*

§*Interdisciplinary Center for Scientific Computing (IWR), Heidelberg University, Heidelberg*

E-mail: csteine@gwdg.de; frauke.graeter@h-its.org

SI Methods

Preparation of the ezrin-FERM-membrane starting complex.

To assemble the ezrin-FERM-membrane complex, serving as the starting point of all ezrin-FERM simulations, we exploited the high sequential and structural similarity between the ezrin-FERM structure (PDB accession code 4RMA;[1] solved through x-ray diffraction at a resolution of 1.7 Å) and the radixin-FERM-inositol-(1,4,5)-triphosphate complex (PDB accession code 1GC6;[2] solved in x-ray diffraction at a resolution of 2.9 Å). The ezrin-FERM-membrane starting structure was produced in the following way:

1. A preliminary PIP_2-containing 'helper membrane' was generated using the web interface of the CHARMM-GUI Membrane Builder.[3,4] It solely served as a full-length PIP_2 source and orientation reference.

2. Structural alignment of the radixin-FERM-inositol-(1,4,5)-triphosphate complex and the helper membrane based on the coordinates of a PIP_2 approximately located at the center of the helper membrane and the coordinates of the inositol-(1,4,5)-triphosphate molecule within the radixin-FERM-inositol-(1,4,5)-triphosphate complex. This was accomplished using the alignment capabilities of UCSF Chimera.[5]

3. Removal of protein-membrane clashes introduced in step 2 by alternate application of small-angle rotations and translations in z-direction (orthogonal to the membrane) to the radixin-FERM-PIP2 complex (realized in VMD[6]).

4. Structural alignment of the ezrin-FERM domain with the radixin-FERM-PIP2 complex (realized in VMD).

5. Clashfree generation of a new membrane around the PIP2-molecule that was docked to the pre-oriented ezrin-FERM-PIP2 complex.

The sequence analysis tool EMBOSS-NEEDLE[7] computes a sequence similarity of $\sim 96\%$ and sequence identity of $\sim 86\%$ based on the amino acid sequences belonging to the selected FERM domain structures of ezrin and radixin. The minimal RMSDs for the inositol-(1,4,5)-triphosphate-PIP2 fit and the ezrin-radixin FERM fit were 1.35 Å and 0.66 Å, respectively. After solvation and addition of sodium and chloride ions at the target concentration of 150 mM the ezrin-FERM simulation system comprised 127557 atoms.

Preparation of the FAK-FERM-membrane starting complex.

The FAK-FERM-membrane complex was assembled in a similar way from the FAK-FERM structure (PDB accession code 6CB0;[8] solved through x-ray diffraction at a resolution of 1.97 Å) and a previously modeled FAK-dimer-PIP2 complex based on a cryo-EM structure of an FAK-dimer (resolution ~ 6 Å) that was subjected to a PIP_2 docking procedure.[9] The FAK-FERM-membrane complex used for all FAK-FERM simulations was built in three steps:

1. Alignment of the FAK-FERM domain with the FERM domain of one of the FAK-monomers comprising the above-mentioned FAK-dimer (realized in VMD).

2. Cutting out of the coordinates of the superimposed FAK-FERM domain (residues 31 to 375) plus the PIP_2-molecule docked at this side of the FAK-dimer.

3. Assembly of the FAK-FERM-membrane complex by uploading the structure obtained in step 2 to the CHARMM-GUI Membrane Builder (analogously to step 5 of the complex assembly for ezrin).

After solvation and addition of sodium and chloride ions at the target concentration of 150 mM the FAK-FERM simulation system comprised 171301 atoms.

Production runs

The interaction of the ezrin- and FAK-FERM domains with the PIP_2-containing lipid bilayers was simulated for 8.1 μs and 6.9 μs in 10 independent replicates, respectively. The precise duration of each replicate is provided in Table S1. During these production runs lipid and protein coordinates were written every 40 ps. To save disk storage, the coordinates of ions (and water), however, were written only once every 10 ns. While this amount of sampling was sufficient for most of analysis performed in this study, it was not sufficient for an appropriate sampling of differently sized PIP_2-clusters required for the intended evaluation of cluster-

wise charge (Figure 4C of main text). For this reason, 6 replicates per FERM domain were continued for 100 ns writing lipid, protein and ion coordinates once every 10 ps.

Table S1: Simulation data overview. The durations of the individual replicates in ns are compiled for both simulation systems. The first six replicates of simulation systems (marked with a "*") were continued for further 100 ns, with more frequent coordinate write-out of the lipid, protein and ion coordinates.

Replicate	1*	2*	3*	4*	5*	6*	7	8	9	10
Ezrin-FERM	900	800	800	800	800	800	800	800	800	800
FAK-FERM	756.12	649.56	791.68	695.52	697.68	686.6	687.44	643.2	648.44	646.6

Although the simulation systems were well adjusted to the target temperature $T = 303\,\mathrm{K}$ and pressure $p = 1\,\mathrm{bar}$ upon completion of the 6-step CHARMM equilibration protocol of $\sim 1.1\,\mathrm{ns}$ duration, the systems have not yet reached an equilibrium state in the sense that quantities characterizing the FERM-PIP_2 interaction have stabilized. Contact maps, encoding the interaction between the FERM domains and PIP_2-molecules in the simulation systems, make for a reasonable measure to quantitatively assess equilibration on the basis of stabilization of FERM-PIP_2 contact formation. We therefore used the contact analysis tool ConAn[10] to determine the number of contacts for each residue-lipid pair. From these contact maps, we computed the stoichiometry as well as the RMSD between the contact map at time t and the initial contact map ($t = 0$),

$$\mathrm{RMSD}_{\mathrm{cmap}} = \|\mathrm{M(t)} - \mathrm{M(t=0)}\|_{\mathrm{Frobenius}}\,, \tag{1}$$

to compute the development of the contact map RMSD over time for each replicate (Figure S1).

Based on these contact map RMSD time series we decided to conservatively omit the first 600 ns of the each ezrin-FERM replicate (Figure **??**A) and the first 450 ns of each FAK-FERM replicate (Figure **??**B) from data analysis. The equilibrated portion of the simulation data thus amounts to 2.1 μs and 2.4 μs for the ezrin- and FAK-FERM domains. To ensure that the remaining simulation time for each replicate is sufficient we determined the residence

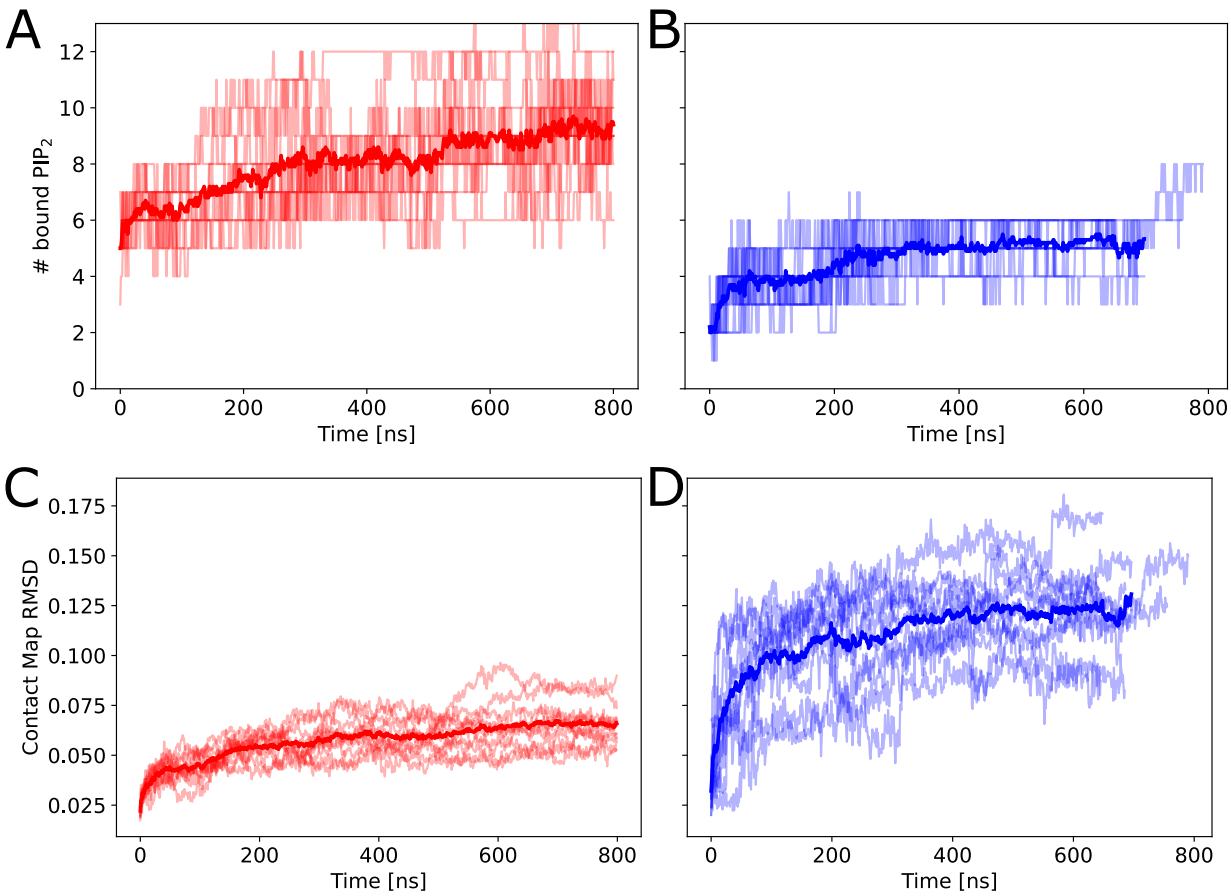

Figure S1: Progression of contacts over time. The upper panel (A,B) shows how the number of bound PIP_2s increases initially. The lower panel (C,D) displays the contact map RMSD with respect to the initial frame of each simulation. Left panels (A,C) represent data for the ezrin-FERM, right panel (B, D) for the FAK-FERM domain. The thin lines represent time series of the individual replicates. Thick lines mark average time series computed from 10 replicates per FERM domain. The time step of RMSD calculation is $\Delta t = 1\,\mathrm{ns}$.

times of each PIP_2 lipid at the FERM domains (Fig. S2). We considered the time the lipids were bound to at least one protein residue. Thus, we only capture unbinding events if a PIP_2 molecule leaves the FERM-membrane interface entirely, but miss unbinding events in the case that PIP_2 immediately binds to another protein residue. The latter likely occurs at the center of the interfaces due to the large amounts of basic residues located there (Fig. 4) and likely amounts for the few observed long residence times spanning large parts of the overall simulation time. However, the vast majority of PIP_2 moleculess stays bound to protein residues for less than 100 ns. Therefore, we conclude that our simulations were conducted for a long enough time despite the large portion discarded for equilibration purposes.

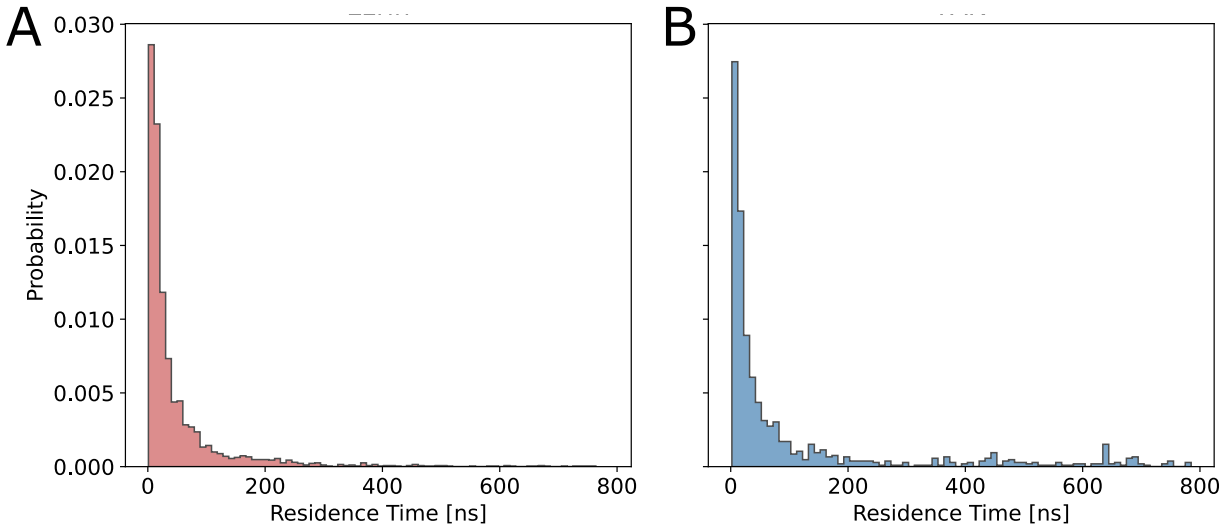

Figure S2: Distribution of PIP_2 residence times at (A) the ezrin-FERM and (B) the FAK-FERM domain.

FERM Domain Positional Variations on the Membrane Surface

To evaluate whether the two FERM domains stayed in their upright position or whether they used potential additional PIP_2 binding sites, we analyzed the angle formed between the protein and the membrane surface (Fig. S3). The angle time traces show fluctuations around 90°, revealing that both FERM domains remain upright albeit with extensive rocking

motions.

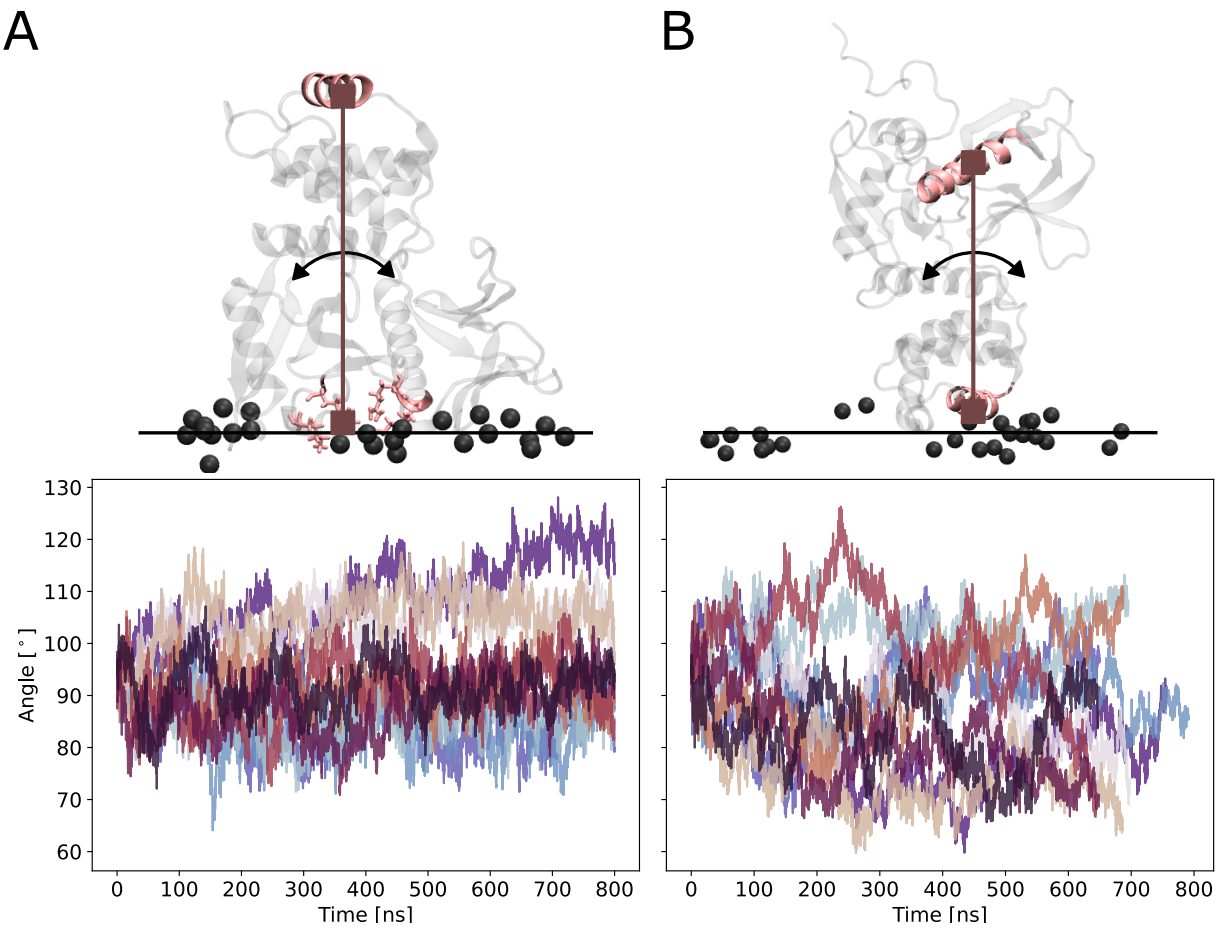

Figure S3: Angle between the membrane located in the xy-plane (black line) and the FERM domain (grey). The top panel illustrates an exemplary simulation frame for each protein. The residues used to define the protein positional vectors (dark pink line) are highlighted in light pink. Black spheres depict the phosphate groups of PIP_2's inositol ring. Each colored line in the bottom panel represents an individual simulation replicate. (A) For ezrin, the vector describing the position of the FERM domain is defined by the basic cleft (COM of residues 60, 63, 278 and 279) and a helix on top of the F2 lobe with respect to the membrane (COM of residues 167-178). (B) The positional vector for FAK is given by the basic patch helix (COM of residues 216-230) and the F3-lobe helix (COM of residues 334-352).

Evaluation of FERM-PIP_2 stoichiometry

Taking into account that the negative charge on a PIP_2 head group is carried by its 4', 5'- and 1'-phosphates (Figure S4), we took a "phosphate-centered" approach when counting the number of PIP_2-molecules bound to a FERM domain at a given time. That is, we considered a PIP_2-molecule to be bound to a FERM domain if the center of one of its phosphate groups, described by the respective position of its P4, P5 or P phosphorus atom, got within 6 Å of the protonated end of a lysine or arginine residue on the FERM domain. Considering the assignment of partial charges according to the CHARMM topology, we assumed the protonated ends to approximately sit at the NZ nitrogen atom for lysines, and at the center between the NH1 and NH2 nitrogen atoms of the guanidium group of arginines (Figure S4).

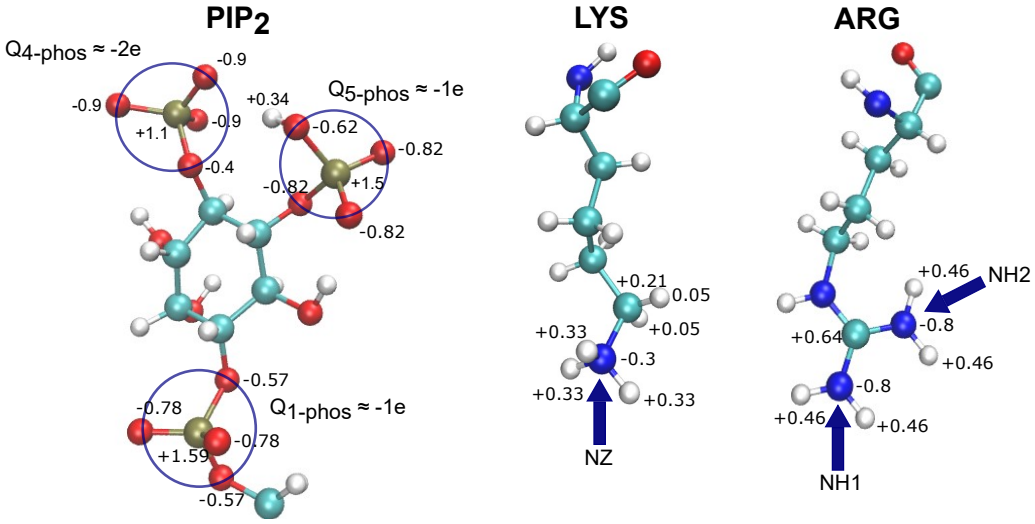

Figure S4: Partial charge assignment. The atoms of a PIP_2 head group, lysine and arginine are labeled according to their partial charges in units of the elementary charge e as defined by the CHARMM topology. Oxygen, phosphorus, carbon, hydrogen, and nitrogen are colored in red, tan, light blue, white and dark blue, respectively. The phosphate groups of the PIP_2-molecule are indicated by blue circles. The partial charges of the labeled atoms at the ends of the lysine and arginine roughly sum to $+1e$. Please note that the relative sizes of the displayed molecules are not true to scale.

The above-mentioned distance cutoff of 6 Å was inferred from the radial distribution functions (RDFs) of the different PIP_2-phosphates around the protonated ends of the lysine and arginine residues (Figure S5C). It was chosen such that secondary peaks reflecting weaker

interaction of 4'-phosphates with lysines/arginines would also be considered when counting the number PIP_2-molecules bound to the FERM domain.

The RDFs were calculated with the GROMACS function *gmx rdf*.[11] Given a selection set

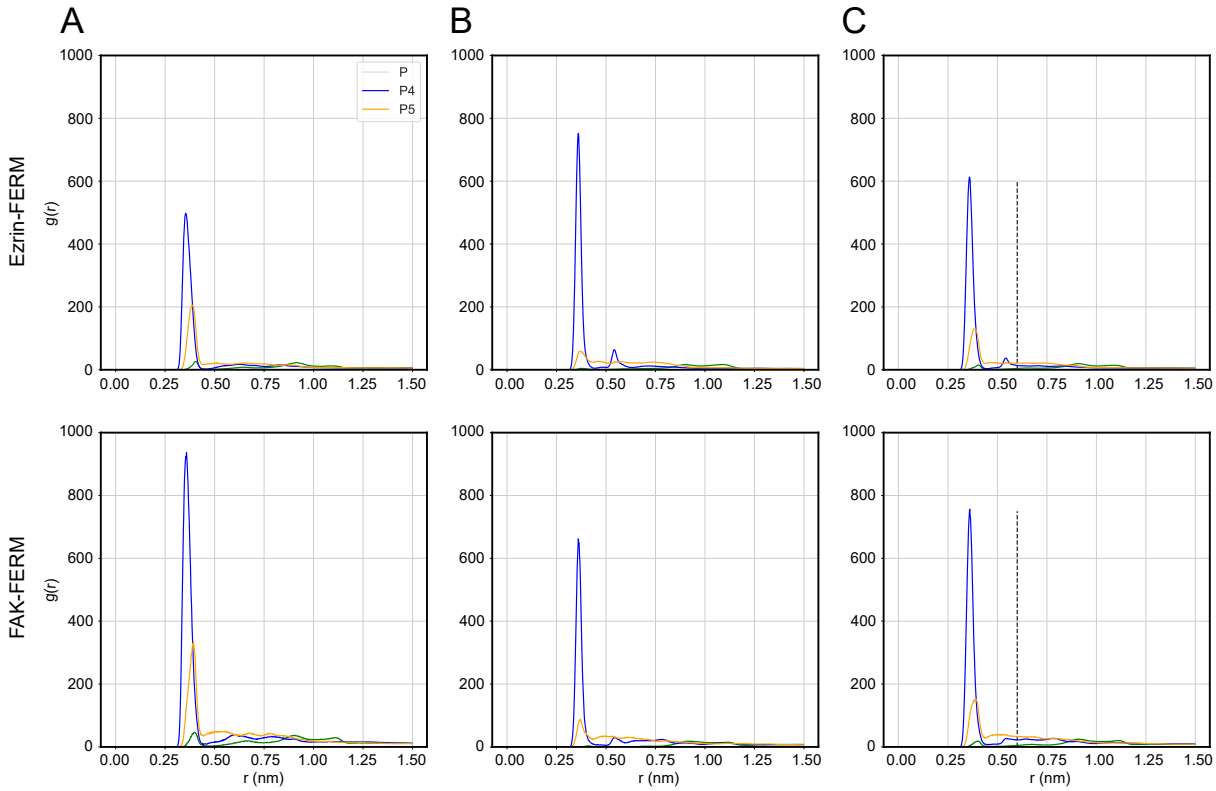

Figure S5: Radial distribution functions of PIP_2-phosphates around lysines and arginines. From left to right the 1-, 4- and 5-phosphate distributions around the lysine NZ-atoms (A), the arginine NH1-/NH2-atoms (B) and the whole set of NZ-/NH1-/NH2-atoms (C) are plotted. The upper and lower panels distinguish between the ezrin and FAK binding poses. The 4-phosphate, 5-phosphate and 1-phosphate RDFs are colored in blue, orange and green, respectively. The RDF curves shown represent averages across the 10 replicates simulated in NaCl per binding pose. For the RDF calculation a maximal sphere size of $r_{\max} = 1.5\,\text{nm}$ and shell thickness of $\Delta r = 0.002\,\text{nm}$ were specified. The lysine and arginine residues included into the RDF calculations were selected after a first rough analysis of contacts within the rather large interaction cutoff of 0.9 nm. A particular lysine/arginine was included when it was observed at least once within the required interaction range. The vertical black dashed line indicates the distance cutoff below which a phosphate was considered to stably interact with a protonated lysine/arginine end.

of atoms B and a reference set of atoms A, *gmx rdf* computes the RDFs of B-atoms around

A-atoms according to

$$g_{\mathrm{AB}}(r) = \frac{\langle n_B(r) \rangle}{\langle n_B \rangle_{\mathrm{local}}} = \frac{1}{\langle n_B \rangle_{\mathrm{local}}} \frac{1}{\mathrm{N_A}} \sum_{\mathrm{i \in A}}^{\mathrm{N_A}} \sum_{\mathrm{j \in B}}^{\mathrm{N_B}} \frac{\delta\left(r_{\mathrm{ij}} - r\right)}{4\pi r^2}, \tag{2}$$

where $\langle n_B \rangle$ denotes the average number density of B-atoms at distance r from A-atoms and $\langle n_B \rangle_{\mathrm{local}}$ represents the number density of B-atoms as averaged over all spheres of radius r_{max} around the A-atoms. In reality, GROMACS calculates an RDF histogram by counting the number of selection set atoms (B-atoms) found in spherical shells of default thickness $\Delta r = 0.002\,\mathrm{nm}$ around the reference set atoms (A-atoms) up to the above-mentioned maximal distance, which is defined by the user. This count is then divided by the number of reference atoms $\mathrm{N_A}$, the shell volume $4\pi r^2 \Delta r$ and the average particle density of the selection atoms $\langle n_B \rangle_{\mathrm{local}}$, rendering $g_{\mathrm{AB}}(r)$ a dimensionless function. When given an entire trajectory *gmx rdf* will also average across the frames comprising the trajectory.

For the computation of the RDFs of the $\mathrm{PIP_2}$-phosphate groups around the lysine and arginine residues of the FERM domain, we chose as representative selection sets

$$\mathrm{B} \in \left\{ \underbrace{\left\{P^{(1)}, \ldots, P^{(\mathrm{N_{PIP2}})}\right\}}_{\text{1-phosphate}}, \underbrace{\left\{P_4^{(1)}, \ldots, P_4^{(\mathrm{N_{PIP2}})}\right\}}_{\text{4-phosphate}}, \underbrace{\left\{P_5^{(1)}, \ldots, P_5^{(\mathrm{N_{PIP2}})}\right\}}_{\text{5-phosphate}} \right\}, \tag{3}$$

marking the centers of the 1-, 4- or 5-phosphate groups of all $\mathrm{N_{PIP2}} = 13$ $\mathrm{PIP_2}$-molecules in the system. To represent the lysine and arginine residues that served as the references for the RDF calculation, we used the atom reference sets

$$\mathrm{A} \in \left\{ \underbrace{\left\{NZ^{(1)}, \ldots, NZ^{(\mathrm{N_{LYS}})}\right\}}_{\text{LYS}}, \underbrace{\left\{NH1^{(1)}, NH2^{(1)}, \ldots, NH1^{(\mathrm{N_{ARG}})}, NH2^{(\mathrm{N_{ARG}})}\right\}}_{\text{ARG}}, \right.$$
$$\left. \underbrace{\left\{NZ^{(1)}, \ldots, NZ^{(\mathrm{N_{LYS}})}, NH1^{(1)}, NH2^{(1)}, \ldots, NH1^{(\mathrm{N_{ARG}})}, NH2^{(\mathrm{N_{ARG}})}\right\}}_{\text{LYS + ARG}} \right\}, \tag{4}$$

where the atoms NZ, NH1 and NH2 as shown in Figure S4, mark the approximate locations of the positive charges carried by the lysine and arginine residues. Note that by specifying the two nitrogen atoms NH1 and NH2 in the reference atom sets for arginine, we do not double the RDF-counts for arginines as compared to the RDF counts for lysine because the RDF as defined in equation (2) is normalized by the number of atoms in the reference set.

Counting in this way the number of PIP_2-molecules bound to the FERM domains for each frame of the equilibrated portion of the simulated trajectories allowed to compute normalized histograms of stoichiometry for both FERM domains (Figure 2A/B of the main text). Based on these discrete probability distributions, mean and standard deviation (STD) were calculated according to

$$\bar{N} = \sum_{\mathrm{n}=\mathrm{n}_{\min}}^{\mathrm{n}_{\max}} p_{\mathrm{n}} n \tag{5}$$

$$\sigma_{\bar{N}} = \left(\sum_{\mathrm{n}=\mathrm{n}_{\min}}^{\mathrm{n}_{\max}} p_{\mathrm{n}} (n - \bar{N})^2 \right)^{1/2}, \tag{6}$$

leading to the values

$$\bar{\mathrm{N}}_{\mathrm{pip2}} = \begin{cases} 7.4 \pm 1.3 & \text{for the ezrin-FERM binding pose} \\ 4.6 \pm 0.8 & \text{for the FAK-FERM binding pose} \end{cases}.$$

reported in the main text.

Contact Analysis

Analysis of residue-wise FERM-PIP_2 contacts and the contributions of FERM-PIP_2 contacts to the overall FERM-membrane contacts was performed with ConAn. Precisely, in what is called the "asymmetric mode", designed for the analysis of inter-molecular interactions, we

ran ConAn on the concatenation of the equilibrated portions of the MD trajectories.
For determination of residue-wise FERM-PIP_2 contacts we peformed three such runs, specifying as the two molecule groups the residue ID range capturing the 13 PIP_2-molecules in the system and

1. ... residues 2 - 86 corresponding to the F1-lobe of the ezrin-FERM domain
2. ... residues 204 - 297 corresponding to the F3-lobe of the ezrin-FERM domain
3. ... residues 180 - 227 corresponding to the F2-lobe of the FAK-FERM domain.

The parameters $d_{\text{inter}} = 0.4\,\text{nm}$ and $d_{\text{high}} = 0.6\,\text{nm}$ introduced in the methods section of the main text correspond to the ConAn input parameters "TRUNC_INTER" and "TRUNC_INTER_HIGH".
To estimate the contribution of FERM-PIP_2 contacts to the overall number of contacts formed between the FERM domains and the membrane, the above asymmetric runs were repeated, this time including also the POPC-molecules of the protein-proximal membrane leaflet into the contact analysis.

Charge compensation analysis

Our analysis of charge compensation in the FERM-membrane interaction interface and on the level of PIP_2-clusters includes charges contributed by lysine and arginine residues, sodium and chloride ions and PIP_2-molecules considered to be in interaction based on distance criteria as explained below. Taking into account the five theoretically possible types of intermolecular hydrogen bond formation between adjacent PIP_2-molecules, 4/5-phosphate-4/5-phosphate, 4/5-phosphate-hydroxyl, hydroxyl-hydroxyl, 4/5-phosphate-1-phosphate, and hydroxyl-1-phosphate,[12] our criterion for clustering PIP_2-molecules together was to require at least one oxygen-oxygen encounter of adjacent PIP_2-molecules within $r_{\text{O}-\text{O}} \leq 0.33\,\text{nm}$, which proved to capture hydrogen bonding well in previous MD study on PIP_2-clustering.[13]

(i) Computation of ion concentration profiles

To compute concentration profiles for the sodium and chloride ions, the simulation system was cut into n slices of thickness $\Delta z = 0.25\,\mathrm{nm}$ along the z-direction, i.e. orthogonal to membrane plane. The ion concentration profiles $c_{\mathrm{Na^+}}(z)$ and $c_{\mathrm{Cl^-}}(z)$ were then computed from the trajectory counts $\mathrm{N}_{\mathrm{ion}}^{(\mathrm{i})}(z)$, $\mathrm{i} = 1, \ldots, \mathrm{n}$ of both ion species in the different slices via

$$c_{\mathrm{ion}}(z) = \frac{1}{\mathrm{n}} \sum_{\mathrm{i}=1}^{\mathrm{n}} \frac{\mathrm{N}_{\mathrm{ion}}^{(\mathrm{i})}(z)}{\mathrm{N_A} A \Delta z}, \tag{7}$$

where $\mathrm{N_A}$ and A denote Avogadros's number and the slice area respectively (Figure S6).

The concentration profiles represent averages across the above-mentioned 6 x 100 ns simulation bits with higher coordinate write-out frequency appended to the first six replicates for each binding pose. For reference, also the mass densities of both FERM domains reflecting the characteristic orientations of the two FERM-domains with respect to the plasma membrane are plotted. In both simulation systems the ion concentration far from the membrane settled at $c_0 = 200\,\mathrm{mM}$ and also the peak sodium concentrations, reached at the approximate average z-coordinate of the PIP_2 head groups, was similar.

(ii) Charge compensation in the FERM-membrane interaction interface

The minutiae of the analysis of the total charge in the FERM-PIP_2 interaction interface are described next. Since the system was prepared to be overall charge-neutral, enlarging a search volume around the PIP_2-molecules checked for charge neutralization must at some point yield a neutral net charge. We thus had to make a choice for the size of the search volume that adequately reflects the zone of FERM-PIP_2 interaction. We defined the search volume as follows:

1. Identify all positively charged protein residues and PIP_2-molecules that form phosphate-lysine/arginine contacts in the above sense.

2. Enlarge search spheres of radius $\mathrm{r_{sph}}$ around the protonated ends of the lysines/arginines

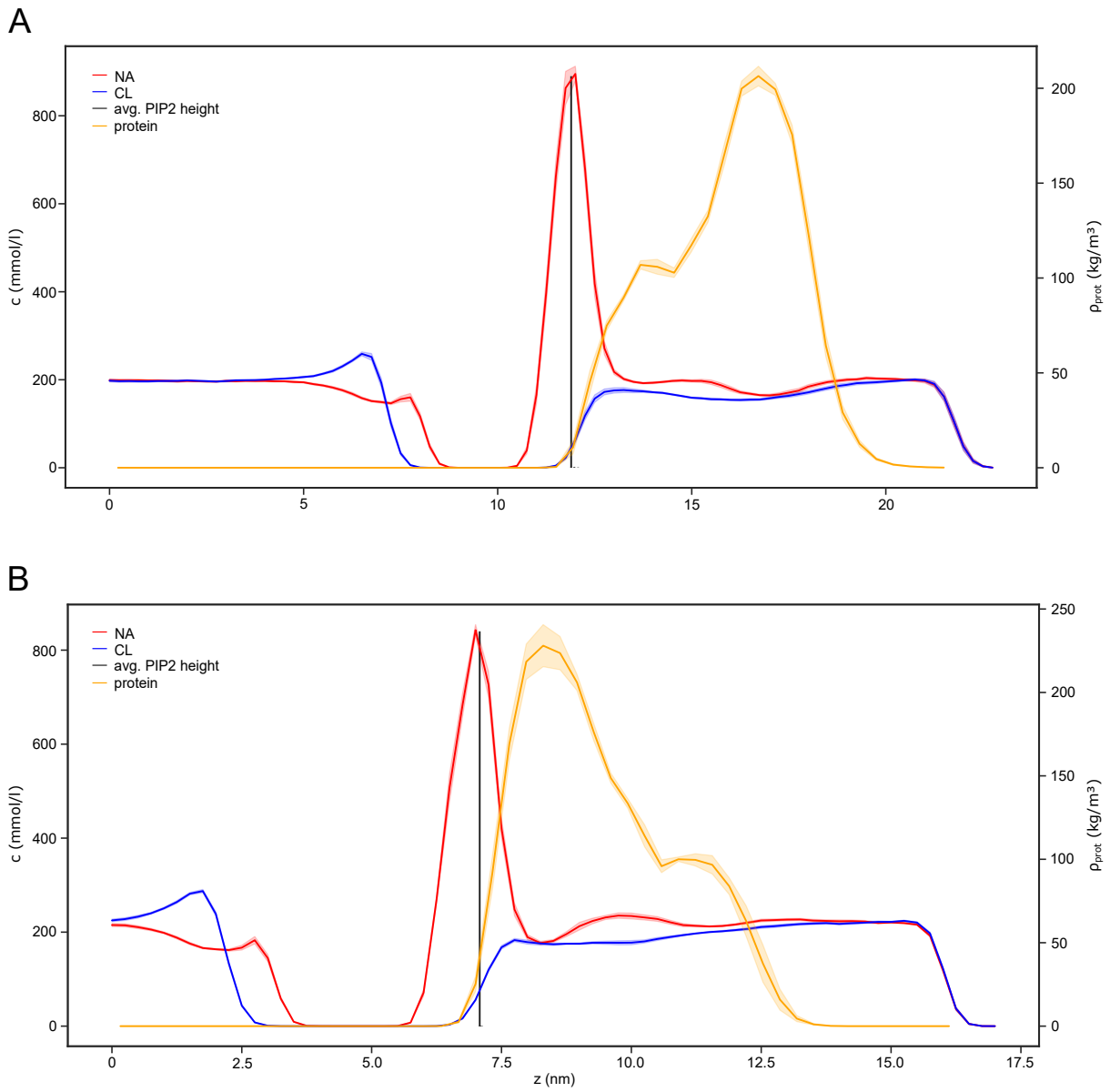

Figure S6: Ion concentration profiles of sodium and chloride along the z-direction computed from (A) the FAK-FERM simulations, and (B) the ezrin-FERM simulations. The profiles for sodium (red) and chloride (blue) represent averages across the above-mentioned 6 x 100 ns simulation bits with higher coordinate write-out frequency appended to the first six replicates for each binding pose. The shaded areas mark the standard deviation zones. For reference, the mass density profiles of both proteins are plotted in orange.

and search for chloride ions.

3. Enlarge search spheres of radius r_{sph} around the P-, P4- and P5-atoms at the centers of the PIP_2-phosphates and search for sodium ions.

4. Add the charges of protein residues and PIP_2-molecules in contact, the charges of chloride ions from 2. and the charges of the sodium ions from 3. to obtain Q_{tot}.

Evaluating time-averages of the total charge found according to the above procedure for the 10 repeat simulations available per binding pose, one obtains 10 independent Q_{tot}-values per binding pose, from which we calculated a global mean and standard deviation of the mean. This calculation was repeated for different search sphere radii between 0.5 nm and 1.0 nm (Figure S7).

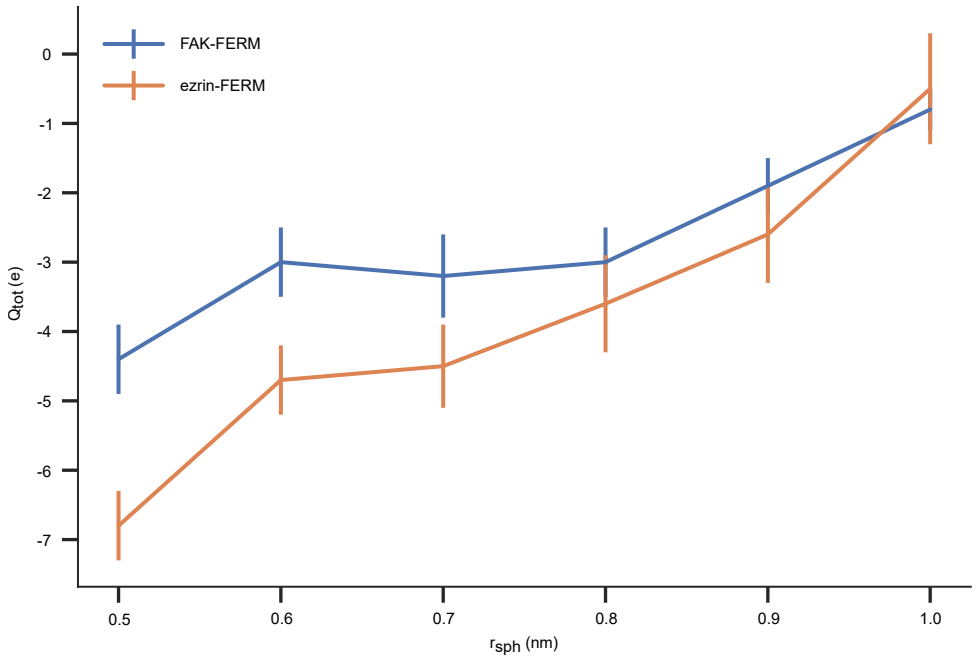

Figure S7: Total interface charge as a function of the search sphere radius.

Evaluating $Q_{tot}(r_{sph})$ at our previously defined cutoff $r_{cut} = 0.6$ nm for phosphate-lysine/arginine interaction, with the idea to include only stably interacting charges into the total charge calculation, yields total interface charges of $Q_{tot}^{ezr}(r_{cut}) \approx -5e$ and $Q_{tot}^{FAK}(r_{cut}) \approx -3e$ for the ezrin- and FAK-FERM domains as reported in the main text of the paper. As ex-

pected, $Q_{\mathrm{tot}}(\mathrm{r_{sph}})$ approaches zero as $\mathrm{r_{sph}}$ is increased. The observation of a slightly negative charge excess in the binding interface zone persists, however, in the intermediate range $\mathrm{r_{sph}} \in \{0.6, 0.7, 0.8, 0.9\}$ nm.

(iii) Charge compensation of PIP_2-molecules and clusters

To analyze charge compensation more locally on the level of individual PIP_2-molecules or clusters, we divided the 13 PIP_2-molecules present in both systems at each frame of the 6 x 100 ns simulation bits per binding pose with higher coordinate write-out frequency into clusters. To this end we deployed the hierarchical single-linkage clustering algorithm, using as a linking criterion an oxygen-oxygen encounter within a distance of $r_{\mathrm{O-O}} \leq 0.33\,\mathrm{nm}$, representing inter-molecular hydrogen bonding. To evaluate the total charge of a PIP_2-cluster we proceeded similarly to the protocol for evaluating charge compensation in the FERM-membrane interface. Precisely, total charge on the cluster level was computed by:

1. identifying the cluster size,
2. counting the number of sodium ions, chloride ions, or protonated ends of lysines/arginines within a distance of $\mathrm{r_{sph}}$ of the phosphate groups of the PIP_2-molecules constituting the cluster, and
3. adding the thus collected charges to the charge $Q_{\mathrm{clust}} = \mathrm{N_{pip2}} * (-4e)$ carried by the $\mathrm{N_{pip2}}$ PIP_2-molecules in the respective cluster.

As for the analysis of the total interface charge in the previous paragraph, we set $\mathrm{r_{sph}} = 0.6\,\mathrm{nm}$.

(iv) Sodium ions substantially aid compensation of PIP_2 charge.

As PIP_2-molecules were simulated with a net charge of $-4\,e$ per molecule, reflecting the

experimentally determined[12] PIP_2 net charge at pH 7.0, the rather high average binding counts we observed for the ezrin- and FAK-FERM domains correspond to a negative charge of $\sim -30\,e$ for the ezrin-FERM domain and $\sim -18\,e$ for the FAK-FERM domain. By contrast, the number of positively charged FERM residues in pronounced interaction ($\bar{n}_{res} \geq 0.5$ avg. contacts/frame) with PIP_2 amounts to only 15 for the ezrin-FERM domain and 7 for the FAK-FERM domain (Figure 4E/F). Consequently, the bound PIP_2-molecules clearly overcompensate the protein surface charges by approximately $-10\,e$ to $-15\,e$. Given this considerable excess of negative charge, the question arises if and how it is compensated to avoid a potential destabilization of FERM-membrane binding. Sodium concentration is maximal at the mean height of the PIP_2-headgroups (Figure S6), suggesting that sodium ions might enter the FERM-membrane binding interface. Chloride concentration, on the other hand, quickly decays toward the lipid bilayer and due to the comparatively large size of the chloride ions is strongly suppressed in the binding interface. To quantify the contribution of sodium ions in the compensation of PIP_2 charge, we decomposed the total charge in the binding interface into its different contributions (Figure S8B). The total interface charge was computed as the sum of protein, PIP_2, sodium and chloride charges.

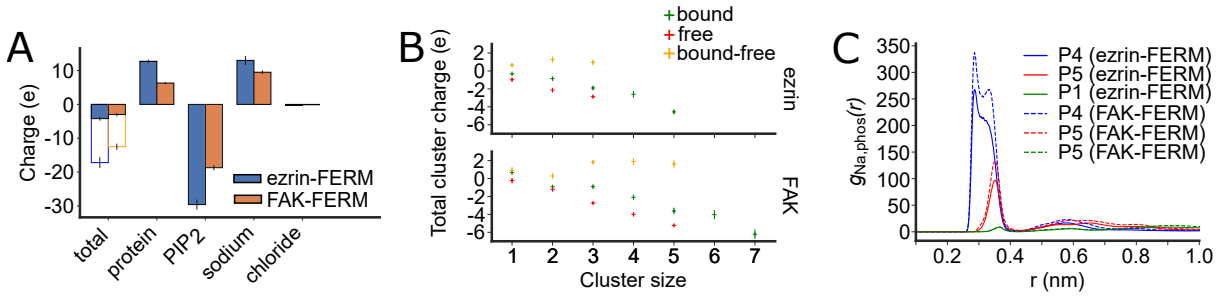

Figure S8: Sodium aids the compensation of PIP_2 charge in the binding interface and on the level of individual PIP_2-clusters. (A) Decomposition of total interface charge. Error bars denote standard errors of the mean computed from $n = 10$ replicates per FERM-domain. (B)Total charge of PIP_2-clusters as a function of cluster size. Error bars denote standard errors of the mean obtained in block averaging. (C) Radial distribution of sodium around phosphorus atoms at the center of the 1'-, 4'- and 5'-phosphate groups of PIP_2.

Scrutinizing the total interface charge in this manner, we find the large amount of negative charge carried by the PIP_2-molecules reduced to $-5\,e$ and $-2\,e$ in the ezrin-FERM

and FAK-FERM simulations due to positive FERM residues and sodium ions contributing positive charge to the interface in roughly equal parts. We hence conclude that sodium ions enter the FERM-membrane binding interface, where they almost completely compensate the excess of negative charge caused by the large stoichiometry of FERM-PIP_2 binding and thus avoid potential destabilization of FERM-membrane binding due to electrostatic repulsion between PIP_2-molecules.

(v) PIP_2 diffusion is electrostatically biased toward positive FERM domain surface. Having found sodium ions to considerably contribute to charge neutralization of the FERM-membrane binding interface and with in principle enough sodium ions in the system to compensate the negative charge of the laterally diffusing PIP_2-molecules, we wondered what drives PIP_2-molecules in such high numbers to the FERM domain surface in the first place. To answer this question we investigated charge compensation of PIP_2-molecules on a more local scale. Taking into account the formation of PIP_2-clusters due to inter-molecular hydrogen bonding,[13] we analyzed the total charge of PIP_2-clusters as a function of cluster size, distinguishing between protein-bound and freely diffusing PIP_2-clusters (Figure S8C). To start with, we note that the average total charge of freely diffusing PIP_2-clusters decreases linearly at a rate of roughly $-1\,e$ per PIP_2-molecule in a cluster. Recalling the net negative charge of PIP_2 to be $-4\,e$, this is only possible when sodium ions and PIP_2-molecules on average associate at a ratio of $\sim$3:1. The radial distribution functions (RDFs) of sodium around the 4'-, 5'- and 1'-phosphate groups of the PIP_2-molecules in the system (Figure S8D) corroborate this reasoning with a double peak in the sodium RDF around the 4'-phosphate and a single peak in the sodium RDF around the 5'-phosphate of PIP_2. Consequently, freely diffusing PIP_2-molecules and clusters, despite their partial neutralization by sodium ions, retain a negative net charge that increases linearly with growing cluster size. This biases lateral diffusion of PIP_2-molecules and clusters toward regions on the FERM domain sur-

face that still excess positive charge in the form of lysine and arginine residues. Calculating the difference between the total charges of protein-bound and freely diffusing PIP_2-clusters (Figure S8C), one finds that upon binding the ezrin- or FAK-FERM domains PIP_2-clusters gain on average $+1\,e$ to $+2\,e$ of charge, which in view of their previous excess of negative charge should be energetically favorable.

Calculation of FERM-Membrane Binding Free Energy

The Gibbs free energy of binding ΔG was calculated using Umbrella Sampling as described previously[14] (Fig. S9). We randomly selected three starting frames for each protein from the equilibrium MD simulations, in which the FERM domains where bound by the average number of PIP_2s. We pulled on the protein backbone and lower leaflet of the membrane in opposite directions with a constant velocity of 0.05 m/s and a spring constant of 500 kJ/mol/nm^2. To avoid shearing of the FERM-domain lobes and removal of individual lipids from the membrane we additionally restrained the distance of the four closest heavy atom pairs between the F1 und F3 lobes with a force constant of 50 kJ/mol/nm^2 and the position of the PIP_2 head groups to the height of the membrane plane with a force constant of 1000 kJ/mol/nm^2. Umbrella sampling windows were extracted from the pulling trajectories with a spacing of 0.1 nm during the first 1 nm distance increase between the center of mass of the protein and lower membrane leaflet and 0.2 nm afterwards to cover a distance of at least 4 nm. We simulated each window for 50 ns and discarded the first 10 ns prior to analysis with the weighted histogram analysis method.[15]

Calculation of protein area coverage and packing parameter

To calculate the area A_{one} covered by each FERM domain, we determined the density of the domains using the Gromaps package[16] and projected these densities onto the membrane

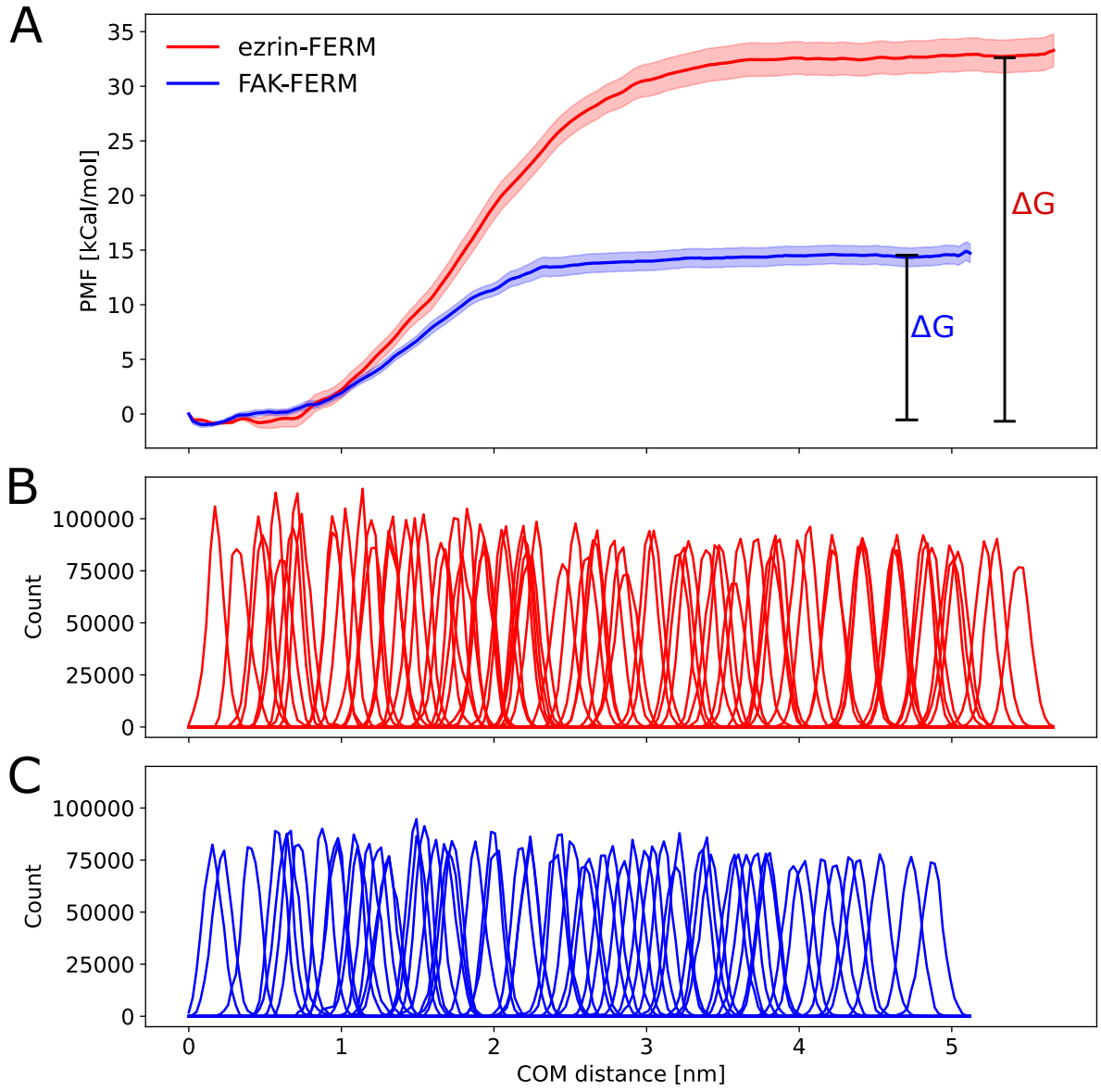

Figure S9: PMF-trace and histograms of Umbrella Sampling calculations. (A) PMF-traces determined by the weighted histogram analysis method. ΔG is calculated as the difference between the lower and upper plateau of the curves. Panels (B) and (C) show the corresponding histograms for ezrin and FAK, respectively.

plane. For estimation of the packing parameter α, we subjected an array of 64 domains to lateral pressure.

$$\alpha = \frac{64 A_{\mathrm{one}}}{A_{\mathrm{Array}}} \tag{8}$$

with A_{Array} being the total area of the protein array.

Model for binding of proteins to multiple surface-bound ligands

The protein has n binding sites and a footprint of A_{P}. The ligand has a footprint of $A_{\mathrm{L}} < A_{\mathrm{P}}$. The area covered by of one FAK-FERM was $A_{\mathrm{one}} = 18.6 \pm 0.9\,\mathrm{nm}^2$ and for ezrin-FERM $A_{\mathrm{one}} = 15.1 \pm 1.0\,\mathrm{nm}^2$ which was divided by the maximal surface coverage ($\alpha_{\mathrm{FAK-FERM}} = 0.73 \pm 0.04$ and $\alpha_{\mathrm{ezrin-FERM}} = 0.50 \pm 0.02$) to get the respective A_{P}. The values for the area covered by one FERM-domain and the maximal surface coverage are derived from the MD simulations.

Protein coverage

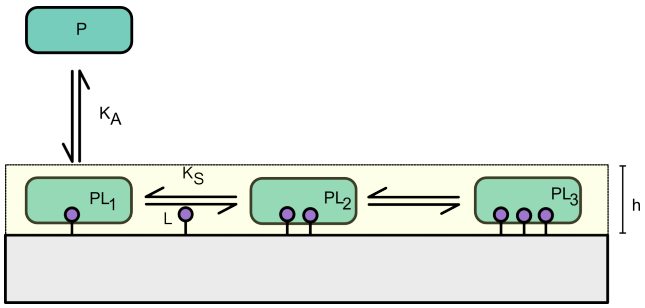

Figure S10: Adsorption of proteins P onto specific sites (ligands L).

Here, we sum only the *occupied* binding sites. The protein may cover 1, 2 or more ligands.

$$\Gamma_{\mathrm{P}} = \frac{N_{\mathrm{P}}}{A} = \Gamma_{\mathrm{PL}_1} + \Gamma_{\mathrm{PL}_2} + ... + \Gamma_{\mathrm{PL_n}} \tag{9}$$

where N_{P} is the number (moles) of protein on the surface of area A. Γ denotes the respective surface concentration.

Conservation of ligands

The number of ligands is constant. Initially, i.e., prior to binding the number was N_{L0}:

$$N_{\mathrm{L0}} = N_{\mathrm{PL}_1} + 2N_{\mathrm{PL}_2} + 3N_{\mathrm{PL}_3} + ... + nN_{\mathrm{PL_n}} + N_{\mathrm{L}} \tag{10}$$

N_{L} is the number of non-bound ligands on the surface. Written in surface concentrations we obtain:

$$\Gamma_{\mathrm{L0}} = \Gamma_{\mathrm{PL}} + 2\Gamma_{\mathrm{PL}_2} + 3\Gamma_{\mathrm{PL}_3} + ... + n\Gamma_{\mathrm{PL_n}} + \Gamma_{\mathrm{L}} \tag{11}$$

Multiple binding reactions

$$\mathrm{PL} + \mathrm{L} \rightleftharpoons \mathrm{PL}_2, \mathrm{PL}_2 + \mathrm{L} \rightleftharpoons \mathrm{PL}_3, \mathrm{PL_{n\text{-}1}} + \mathrm{L} \rightleftharpoons \mathrm{PL_n} \tag{12}$$

The first mass of action reaction with the surface binding constant $K_{\mathrm{S}}[\mathrm{m}^2/\mathrm{mol}]$ reads:

$$K_{\mathrm{S}} = \frac{\Gamma_{\mathrm{PL}_2}}{\Gamma_{\mathrm{PL}}\Gamma_{\mathrm{L}}} \tag{13}$$

The second reaction reads:

$$K_{\mathrm{S}} = \frac{\Gamma_{\mathrm{PL}_3}}{\Gamma_{\mathrm{PL}_2}\Gamma_{\mathrm{L}}} \tag{14}$$

and consequently we find for the last reaction after plugging in all the previous reactions $\Gamma_{\mathrm{PL(n-1)}}$:

$$\Gamma_{\mathrm{PLn}} = (K_{\mathrm{S}}\Gamma_{\mathrm{L}})^{n-1}\Gamma_{\mathrm{PL}_1} \tag{15}$$

Note that the association constant $K_{\mathrm{A}}[\mathrm{m}^3/\mathrm{mol}]$ reads:

$$K_{\mathrm{A}} = \frac{\Gamma_{\mathrm{PL}}}{c_{\mathrm{P}}\Gamma_{\mathrm{L}}} \tag{16}$$

It is possible to transform between two and three dimensions a protein encounters through the simple expression $K(2D) = K(3D)/h$, where h is the confinement length. The basic idea is that if two interacting species are confined to a region of length $h \approx 1 - 10\,\mathrm{nm}$ along an axis perpendicular to the plane of a membrane, then they are effectively confinded to a volume $V = Ah$, where A is the area per molecule. This simple procedure turns a 2D system into a 'quasi-3D system' because there is now a volume associated with each molecule even when it is constrained to a planar membrane. The result is not influenced by the height between $1 - 10\,\mathrm{nm}$. The protein concentration in solution can then be written as:

$$c_{\mathrm{P}} = \frac{N_{\mathrm{P}}}{Ah} = \frac{\Gamma_{\mathrm{P}}}{h} \tag{17}$$

inserting in equation (16) gives:

$$K_{\mathrm{A}} = \frac{\Gamma_{\mathrm{PL}} h}{\Gamma_{\mathrm{P}} \Gamma_{\mathrm{L}}} = h K_{\mathrm{S}} \tag{18}$$

That means if a protein binds to the first ligand it moves into the surface slab, where the second site encounters a higher apparent concentration of ligands. Mathematically this is equivalent to the binding of the first ligand increasing the association constant for the second site.

K_{A} was calculated with the equation $\Delta G = -RT \ln(K_{\mathrm{A}})$ where we inserted the Gibbs free energy change from the MD simulations at 21 °C ($\Delta G_{\mathrm{FAK-FERM}} = -12.4 \pm 2.2\,\mathrm{kcal/mol}$, $\Delta G_{\mathrm{ezrin-FERM}} = -30.5 \pm 4.4\,\mathrm{kcal/mol}$).

Protein concentration on the surface

Plugging equation (15) into the conservation equation (11) we arrive at:

$$\Gamma_{\mathrm{L0}} = \Gamma_{\mathrm{PL}} + \sum_{i=2}^{n} i (K_{\mathrm{S}} \Gamma_{\mathrm{L}})^{i-1} \Gamma_{\mathrm{PL}} + \Gamma_{\mathrm{L}} \tag{19}$$

or

$$\Gamma_{\mathrm{PL}} = \frac{\Gamma_{\mathrm{L0}} - \Gamma_{\mathrm{L}}}{\sum_{i=1}^{n} i (K_{\mathrm{S}} \Gamma_{\mathrm{L}})^{i-1}} \tag{20}$$

and eventually by summing up the expression for $\Gamma_{\mathrm{PL_2}}, \Gamma_{\mathrm{PL_3}} ... \Gamma_{\mathrm{PL_n}}$ plugged into equation (9):

$$\Gamma_{\mathrm{P}} = \frac{(\Gamma_{\mathrm{L0}} - \Gamma_{\mathrm{L}})(1 + K_{\mathrm{S}} \Gamma_{\mathrm{L}} + ... + (K_{\mathrm{S}} \Gamma_{\mathrm{L}})^{n-1})}{\sum_{i=1}^{n} i (K_{\mathrm{S}} \Gamma_{\mathrm{L}})^{i-1}} \tag{21}$$

or

$$\Gamma_{\mathrm{P}} = \frac{(\Gamma_{\mathrm{L0}} - \Gamma_{\mathrm{L}}) \sum_{i=1}^{n} (K_{\mathrm{S}}\Gamma_{\mathrm{L}})^{i-1}}{\sum_{i=1}^{n} i(K_{\mathrm{S}}\Gamma_{\mathrm{L}})^{i-1}} \tag{22}$$

Translating into bound fractions $\Theta_{\mathrm{P}} = \Gamma_{\mathrm{P}}/\Gamma_{\mathrm{P}}^{\mathrm{max}} = \Gamma_{\mathrm{P}}(N_{\mathrm{A}}A_{\mathrm{P}})$ since $\Gamma_{\mathrm{P}}^{\mathrm{max}} = 1/(N_{\mathrm{A}}A_{\mathrm{P}})$:

$$\Theta_{\mathrm{P}} = A_{\mathrm{P}}N_{\mathrm{A}}(\Gamma_{\mathrm{L0}} - \Gamma_{\mathrm{L}}) \frac{\sum_{i=1}^{n} (K_{\mathrm{S}}\Gamma_{\mathrm{L}})^{i-1}}{\sum_{i=1}^{n} i(K_{\mathrm{S}}\Gamma_{\mathrm{L}})^{i-1}} \tag{23}$$

Figure S11 shows the input data of the procedure for the FAK-FERM derived from experimental data from which the free PIP_2 concentration (ligand) was calculated with an assumed stoichiometry of $n = 2$ and $n = 3$. If $n = 2$ is increased to $n = 3$, the free PIP_2 concentration reaches values below zero indicating that all protein bindings sites are occupied.

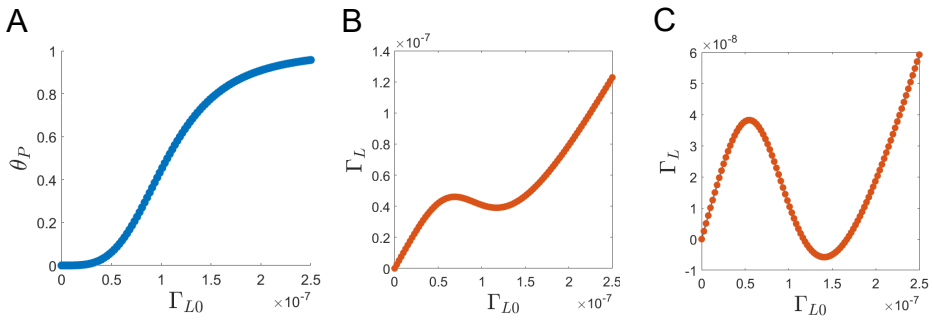

Figure S11: Simulation of free PIP_2 concentration. (A) Input data - FAK-FERM coverage as a function of surface concentration of PIP_2. (B) Free ligand concentration as a function of PIP_2 content with an assumed stoichiometry of $n = 2$. (C) Free ligand concentration as a function of PIP_2 content with an assumed stoichiometry of $n = 3$.

References

(1) Phang, J. M.; Harrop, S. J.; Duff, A. P.; Sokolova, A. V.; Crossett, B.; Walsh, J. C.; Beckham, S. A.; Nguyen, C. D.; Davies, R. B.; Glöckner, C., et al. Structural characterization suggests models for monomeric and dimeric forms of full-length ezrin. *Biochemical Journal* **2016**, *473*, 2763–2782.

(2) Hamada, K.; Shimizu, T.; Matsui, T.; Tsukita, S.; Tsukita, S.; Hakoshima, T. Structural basis of the membrane-targeting and unmasking mechanisms of the radixin FERM domain. *The EMBO journal* **2000**, *19*, 4449–4462.

(3) Jo, S.; Kim, T.; Iyer, V. G.; Im, W. CHARMM-GUI: a web-based graphical user interface for CHARMM. *Journal of computational chemistry* **2008**, *29*, 1859–1865.

(4) Lee, J.; Cheng, X.; Swails, J. M.; Yeom, M. S.; Eastman, P. K.; Lemkul, J. A.; Wei, S.; Buckner, J.; Jeong, J. C.; Qi, Y., et al. CHARMM-GUI input generator for NAMD, GROMACS, AMBER, OpenMM, and CHARMM/OpenMM simulations using the CHARMM36 additive force field. *Journal of chemical theory and computation* **2016**, *12*, 405–413.

(5) Pettersen, E. F.; Goddard, T. D.; Huang, C. C.; Couch, G. S.; Greenblatt, D. M.; Meng, E. C.; Ferrin, T. E. UCSF Chimera—a visualization system for exploratory research and analysis. *Journal of computational chemistry* **2004**, *25*, 1605–1612.

(6) Humphrey, W.; Dalke, A.; Schulten, K. VMD: visual molecular dynamics. *Journal of molecular graphics* **1996**, *14*, 33–38.

(7) Madeira, F.; Park, Y. M.; Lee, J.; Buso, N.; Gur, T.; Madhusoodanan, N.; Basutkar, P.; Tivey, A. R.; Potter, S. C.; Finn, R. D., et al. The EMBL-EBI search and sequence analysis tools APIs in 2019. *Nucleic acids research* **2019**, *47*, W636–W641.

(8) Marlowe, T.; Dementiev, A.; Figel, S.; Rivera, A.; Flavin, M.; Cance, W. High resolution crystal structure of the FAK FERM domain reveals new insights on the Druggability of tyrosine 397 and the Src SH3 binding site. *BMC molecular and cell biology* **2019**, *20*, 1–9.

(9) Goñi, G. M.; Epifano, C.; Boskovic, J.; Camacho-Artacho, M.; Zhou, J.; Bronowska, A.; Martín, M. T.; Eck, M. J.; Kremer, L.; Gräter, F., et al. Phosphatidylinositol 4, 5-bisphosphate triggers activation of focal adhesion kinase by inducing clustering and

conformational changes. *Proceedings of the National Academy of Sciences* **2014**, *111*, E3177–E3186.

(10) Mercadante, D.; Gräter, F.; Daday, C. CONAN: a tool to decode dynamical information from molecular interaction maps. *Biophysical journal* **2018**, *114*, 1267–1273.

(11) Abraham, M.; Van Der Spoel, D.; Lindahl, E.; Hess, B., et al. GROMACS user manual version 5.0. 4. *Sweden: Royal Institute of Technology and Uppsala University* **2014**,

(12) Kooijman, E. E.; King, K. E.; Gangoda, M.; Gericke, A. Ionization properties of phosphatidylinositol polyphosphates in mixed model membranes. *Biochemistry* **2009**, *48*, 9360–9371.

(13) Han, K.; Gericke, A.; Pastor, R. W. Characterization of specific ion effects on PI (4, 5) P2 clustering: molecular dynamics simulations and graph-theoretic analysis. *The Journal of Physical Chemistry B* **2020**, *124*, 1183–1196.

(14) Lemkul, J.; Bevan, D. Assessing the Stability of Alzheimer's Amyloid Protofibrils Using Molecular Dynamics. *Journal of Physical Chemistry B* **2010**, *114*, 1652–1660.

(15) Hub, J. S.; de Groot, B. L.; Van Der Spoel, D. g_{wham} - A free weighted histogram analysis implementation including robust error and autocorrelation estimates. *Journal of Chemical Theory and Computation* **2010**, *6*, 3713–3720.

(16) Briones, R.; Blau, C.; Kutzner, C.; de Groot, B. L.; Aponte-Santamaría, C. GROmaρs: A GROMACS-Based Toolset to Analyze Density Maps Derived from Molecular Dynamics Simulations. *Biophysical Journal* **2019**, *116*, 4–11.